nature cell biology

Bcl-x_L regulates metabolic efficiency of neurons through interaction with the mitochondrial F_1F_O ATP synthase

Kambiz N. Alavian[1,11], Hongmei Li[1,11], Leon Collis[2,11], Laura Bonanni[3], Lu Zeng[1], Silvio Sacchetti[1,4], Emma Lazrove[1], Panah Nabili[1], Benjamin Flaherty[1], Morven Graham[5], Yingbei Chen[6], Shanta M. Messerli[2], Maria A. Mariggio[4], Christoph Rahner[5], Ewan McNay[7], Gordon C. Shore[8], Peter J. S. Smith[2,9], J. Marie Hardwick[6,10] and Elizabeth A. Jonas[1,12]

Anti-apoptotic Bcl2 family proteins such as Bcl-x_L protect cells from death by sequestering apoptotic molecules, but also contribute to normal neuronal function. We find in hippocampal neurons that Bcl-x_L enhances the efficiency of energy metabolism. Our evidence indicates that Bcl-x_L interacts directly with the β-subunit of the F_1F_O ATP synthase, decreasing an ion leak within the F_1F_O ATPase complex and thereby increasing net transport of H^+ by F_1F_O during F_1F_O ATPase activity. By patch clamping submitochondrial vesicles enriched in F_1F_O ATP synthase complexes, we find that, in the presence of ATP, pharmacological or genetic inhibition of Bcl-x_L activity increases the membrane leak conductance. In addition, recombinant Bcl-x_L protein directly increases the level of ATPase activity of purified synthase complexes, and inhibition of endogenous Bcl-x_L decreases the level of F_1F_O enzymatic activity. Our findings indicate that increased mitochondrial efficiency contributes to the enhanced synaptic efficacy found in Bcl-x_L-expressing neurons.

B-cell lymphoma 2 (Bcl2) family proteins regulate programmed cell death[1–3]. In the brain, neurons are eliminated during development, and after insults such as ischaemia, infection or trauma[1–3]. The mechanisms by which anti-apoptotic proteins such as Bcl2 and B-cell lymphoma-extra large (Bcl-x_L) prevent death are incompletely understood. Bcl-x_L sequesters pro-apoptotic members of the Bcl2 family and BH3-only proteins[4–6]. Bcl-x_L also enhances metabolite exchange between mitochondria and the cytosol through interaction with VDAC, helping to prevent the release of death-promoting factors[7].

Bcl-x_L is often highly expressed in cancer cells resistant to cell death, but also functions in neuronal plasticity. Bcl-x_L is the predominant anti-apoptotic protein in the adult brain[8]. Overexpression of Bcl-x_L increases the number and size of synapses, localizes mitochondria to presynaptic sites[9] and increases mitochondrial biomass[10].

As synapses develop and grow, the formation of a larger reserve of neurotransmitter-containing vesicles contributes to more frequent or prolonged synaptic events[11]. The function of these larger pools of synaptic vesicles depends on the metabolism and position of mitochondria at the synapse[12]. Certain mitochondrial-interacting proteins such as Drp1 and Bcl-x_L participate in synaptic strengthening or vesicle recovery after high-frequency firing[3,12–14]. As high metabolic demand occurs during synaptic strengthening, a possible action of Bcl-x_L is to increase the release or production of mitochondrial metabolites during synaptic plasticity.

We have now found that neurons overexpressing Bcl-x_L have higher ATP levels, and cells in which endogenous Bcl-x_L is depleted or inhibited have lower ATP levels. Despite the increase in the level of ATP, neurons overexpressing Bcl-x_L use less oxygen, and Bcl-x_L depletion increases the level of oxygen uptake. In addition to its outer membrane localization, we find Bcl-x_L in the mitochondrial matrix by immuno-electron microscopy. Bcl-x_L co-immunoprecipitates with the β-subunit of the F_1F_O ATP synthase and binds to the purified recombinant β-subunit of the F_1 ATP synthase. Exogenously applied Bcl-x_L increases the level of F_1F_O ATPase activity, and Bcl-x_L inhibition

[1]Department of Internal Medicine, Yale University, New Haven, Connecticut 06520, USA. [2]Biocurrents Research Center, Marine Biological Laboratory, Woods Hole, Massachusetts 02543, USA. [3]Department of Oncology and Neuroscience and Aging Research Center, University G.D'Annunzio of Chieti-Pescara, I-66013 Chieti, Italy. [4]Department of Biochemistry, Physiology and Pathology of Muscle, Basic and Applied Medical Sciences, Università G.D'Annunzio of Chieti-Pescara, I-66013 Chieti, Italy. [5]Department of Cell Biology, Yale University, New Haven, Connecticut 06520, USA. [6]Department of Pharmacology and Molecular Sciences, Johns Hopkins, Baltimore, Maryland 21205, USA. [7]Behavioural Neuroscience and Center for Neuroscience Research, University at Albany, New York 12222, USA. [8]Gemin X Pharmaceuticals, Montréal, Quebec H2X 2H7, Canada. [9]Institute for Life Sciences, University of Southampton, SO17 1BJ, UK. [10]Department of Molecular Microbiology and Immunology, Johns Hopkins, Baltimore, Maryland 21205, USA. [11]These authors contributed equally to the work.
[12]Correspondence should be addressed to E.A.J. (e-mail: elizabeth.jonas@yale.edu)

Received 7 June 2011; accepted 2 August 2011; published online 18 September 2011; DOI: 10.1038/ncb2330

decreases the enzymatic rate. Bcl-x_L deficiency decreases the capacity of F_1F_O-ATPase-containing submitochondrial vesicles to sequester H^+ ions, indicating that Bcl-x_L depletion causes protons to leak following activation of the enzyme. By patch clamping F_1F_O-ATPase-containing vesicles exposed to ATP, we record an increased leak conductance when Bcl-x_L is inhibited or depleted. We therefore suggest a model whereby Bcl-x_L increases the efficiency of ATP synthesis by decreasing a proton leak within the F_1F_O ATPase, thus improving neuronal metabolism.

RESULTS

ATP levels are elevated in Bcl-x_L-overexpressing neurons and decreased in Bcl-x_L-depleted neurons

To determine the effect of Bcl-x_L on ATP levels in neurons, the luminescence intensity of firefly luciferin–luciferase was measured in cultured hippocampal neurons expressing lentivirus constructs for green fluorescent protein (GFP)-tagged Bcl-x_L or control GFP (ref. 15). ATP levels in GFP–Bcl-x_L-expressing cultures were approximately twice that of non-transduced or GFP-expressing controls (Fig. 1a and Supplementary Fig. S1a). Knockdown of Bcl-x_L with an shRNA-carrying lentivirus but not with a scrambled control virus decreased ATP levels (Fig. 1b,c), although the level of cell death was not significantly different at the time of the study (Supplementary Fig. S1b). To further examine the effect of endogenous Bcl-x_L on ATP levels, Bcl-x_L activity was pharmacologically inhibited by ABT-737, a mimetic of BH3-only proteins that binds to Bcl-x_L (refs 14,16). ATP levels were decreased in cultures exposed to ABT-737 (Fig. 1d).

Measurements of luminescence in lysed cells cannot accurately indicate ongoing levels of ATP production in live neurons. Therefore, to measure ATP levels in live neurons (excluding glia), neurons were engineered to express luciferase by lentiviral transduction (Fig. 1d). The application of luciferin led to an immediate rise in luminescence intensity (Fig. 1e calibrated to known concentrations of ATP). Such calibrated light levels were significantly higher in GFP–Bcl-x_L-expressing neurons when compared with mito-GFP controls (Fig. 1f).

Elevated ATP levels in the Bcl-x_L-overexpressing cultures may be explained by an increase in the level of aeorobic glycolysis. To determine whether glycolysis is increased by Bcl-x_L, lactate production was assessed by measuring lactate levels in the medium. The lactate level was significantly higher in controls when compared with the Bcl-x_L-expressing neurons, indicating that Bcl-x_L cells have a lower level of aerobic glycolytic activity than controls (Fig. 1g). To further investigate the use of mitochondrial metabolism, cell viability was measured in a medium containing only mitochondrial substrates (Supplementary Fig. S1c). GFP–Bcl-x_L-overexpressing cells had improved survival when compared with controls, indicating enhanced mitochondrial competence.

Bcl-x_L decreases the level of mitochondrial oxygen uptake

Previous work described increased mitochondrial biomass in neurons overexpressing Bcl-x_L (ref. 10; also see Supplementary Fig. S2). If increased mitochondrial biomass were solely responsible for increased ATP levels, then Bcl-x_L-expressing cells would be expected to have increased oxygen uptake. To examine this, oxygen uptake was measured in single neurons in culture using a sensitive self-referencing oxygen electrode[17] (Fig. 2a and Supplementary Fig. S3a,b). Contrary to expectation, the oxygen flux of Bcl-x_L-overexpressing neurons was lower than that of mito-GFP-transfected neurons (Fig. 2b), indicating that Bcl-x_L-overexpressing neurons couple ATP production more efficiently to oxygen uptake. Endogenous Bcl-x_L has a similar effect because shRNA-mediated depletion (Fig. 2c,d) or pharmacological inhibition of Bcl-x_L (Fig. 2e) activity increased oxygen flux by neurons. These data indicate that depletion or inhibition of Bcl-x_L uncouples ATP production from oxygen uptake[18–20].

The higher ATP levels and lower levels of oxygen uptake of Bcl-x_L-overexpressing neurons may, in theory, result from a quiescent state where ATP accumulates owing to decreased levels of electrical and synaptic activity. This is unlikely because Bcl-x_L-overexpressing neurons have larger synapses and more spontaneous activity than controls[9,10]. Therefore, we investigated whether Bcl-x_L-overexpressing neurons have a greater but underutilized energetic capacity. Bcl-x_L-overexpressing neurons increased their oxygen flux by approximately 90% over the basal level when cells were depolarized with high potassium (high K) conditions, a treatment known to stimulate neuronal electrical and synaptic activity[21,22] (example shown in Fig. 2f), whereas mito-GFP-expressing controls enhanced their flux by only 50%.

During oxidative phosphorylation, protons pumped out of the mitochondrial matrix re-enter the matrix by flux of H^+ across the inner mitochondrial membrane at the ATP synthase (productive flux) and by a H^+ leak (non-productive)[23]. A decrease in the non-productive leak increases the efficiency of ATP production. To determine whether Bcl-x_L-overexpressing neurons have a different degree of non-productive leak across the inner membrane than controls during maximal activity, high K was rapidly washed out of the bath and oxygen uptake was measured in oligomycin, which inhibits H^+ flux associated with ATP production, but does not inhibit H^+ flux associated with the non-productive leak[24]. GFP–Bcl-x_L cells had a higher ratio of productive oxygen flux to total oxygen flux when compared with mito-GFP-expressing controls, indicating that they use a higher percentage of the overall peak oxygen flux to make ATP (Fig. 2g).

Bcl-x_L enhances ATP synthesis during neuronal activity

Neurons may regulate metabolism during periods of increased activity. To study the role of Bcl-x_L in such enhanced energy production, we stimulated neurons with high K conditions and measured the cytosolic ATP levels 5 min after stimulation had ceased. Remarkably, the levels of ATP were increased, indicating a requirement for enhanced energy production that outlasted the period of stimulation. Such an increase in ATP levels was completely prevented by pre-exposure for 5 min of the neurons to the Bcl-x_L inhibitor ABT-737, indicating that Bcl-x_L was specifically required for the stimulation-induced metabolic change (Fig. 2h).

Bcl-x_L is localized to the mitochondrial inner membrane

Most of the previous studies have defined a role for Bcl-x_L in mitochondrial outer membranes as a regulator of cell death or in releasing metabolites from mitochondria[25–29], but a few studies have also indicated a localization of the related anti-apoptotic proteins Bcl2 (refs 30,31) and Bcl-x_L (Hardwick laboratory, unpublished data) to the inner membrane. To confirm and extend these findings, we checked for mitochondrial localization of Bcl-x_L in the Bcl-x_L-overexpressing hippocampal neurons and in control rodent brain using immuno-electron microscopy. Bcl-x_L was localized to the outer membrane

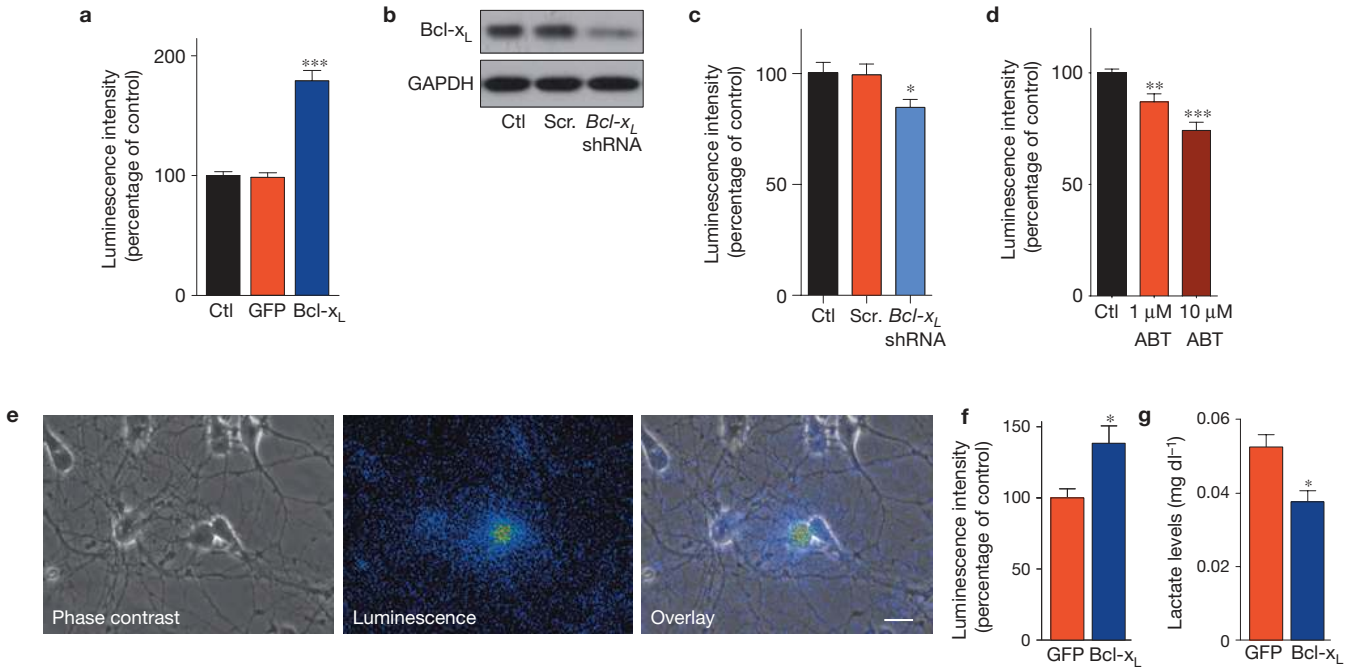

Figure 1 Cellular ATP levels are altered by Bcl-x_L overexpression or depletion in hippocampal neurons. (**a**) ATP levels as measured by firefly luciferin–luciferase luminescence intensity at 7 days after transduction with lentivirus constructs. The luminescence level was normalized to the protein level in each individual well ($N = 8$ wells, $^{***}P < 0.0001$). At least three independent experiments of different cultures showed similar results. Ctl, control. (**b**) Western blot for endogenous Bcl-x_L protein. Cell lysates prepared from non-transduced control hippocampal neuron cultures, scrambled (Scr.)-shRNA-expressing neuron cultures and *Bcl-x_L*-shRNA-expressing neuron cultures at 4 days after viral transduction. GAPDH serves as a loading control. (**c**) ATP levels as measured by firefly luciferin–luciferase luminescence intensity in control cultures or cultures expressing *Bcl-x_L* shRNA or scrambled shRNA at 4 days after viral transduction. The luminescence intensity was normalized to the protein level in each individual well ($N = 11$ for each condition, representing two independent cultures; $^{*}P < 0.03$). (**d**) ATP levels as measured by firefly luciferin–luciferase luminescence intensity in control cultures or cultures exposed for 12–18 h to ABT-737 (ABT) at the indicated concentrations. The luminescence intensity was normalized to the protein level in each individual well ($N = 15$ for each condition, $^{**}P < 0.004$ $^{***}P < 0.0001$, three independent cultures). (**e**) Example image of a neuron expressing a CSCW2–luciferase lentiviral vector. Light is produced in response to the application of 1 mM luciferin. Shown are phase, luminescent and overlay images. In the pseudocolour images, blue is low luminescence and yellow is high luminescence. Scale bar, 20 μm. (**f**) Group data for the amount of ATP represented by the luminescence intensity per coverslip of living hippocampal neurons at 7 days after transfection with the indicated constructs. The light levels were normalized to the average of light levels in mito-GFP control cells. Living neurons were transfected with a CSCW2–luciferase–IG lentivirus vector and mito-GFP or GFP–Bcl-x_L ($N = 8$ coverslips from at least three independent cultures for mito-GFP-expressing neurons, $N = 10$ coverslips from at least three independent cultures of GFP–Bcl-x_L-expressing neurons, $^{*}P < 0.02$). (**g**) Lactate levels in medium surrounding GFP–Bcl-x_L-expressing neurons, compared with GFP-expressing controls, after 12 h in physiological (5 mM) glucose medium (one culture, $N = 3$ replicates for each condition $^{*}P < 0.02$). For all panels error bars indicate s.e.m. Uncropped images of blots are shown in Supplementary Fig. S8.

and inner membrane or matrix of mitochondria of GFP–Bcl-x_L-expressing neurons (Fig. 3a) and native brain mitochondria (Fig. 3b). Furthermore, Bcl-x_L (large gold beads) was co-localized at the inner membrane cristae with a known inner membrane cristae protein, manganese super oxide dismutase[32–34] (MnSOD; small gold beads; Fig. 3b). Overall, Bcl-x_L was localized about equally to inner membrane or matrix and to outer membrane (Fig. 3c). Previous reports indicated localization of the anti-apoptotic protein Bcl2 to the mitochondrial inner membrane[30,31,35] or Bcl-x_L to the same compartment as mitochondrial ATP synthase (Hardwick laboratory, unpublished data). To determine whether Bcl-x_L was indeed localized within this compartment, submitochondrial vesicles of the inner membrane that are enriched in F_1F_O ATP synthase protein complexes (SMVs) and lack an outer membrane were prepared from whole rat brain[36,37]. Bcl-x_L was shown to be present by immunoblot in this purified sample (Supplementary Fig. S4). To further localize Bcl-x_L within the inner membrane, the protein was co-immunoprecipitated with the ATP synthase complex β-subunit using either a specific antibody against Bcl-x_L or a specific antibody against ATP synthase β-subunit (Fig. 3d). To determine the exact binding site of Bcl-x_L, recombinant Flag- and Myc-tagged proteins of the ATP synthase subunits α, β, c, d, δ, ϵ, γ and OSCP were immunoprecipitated from mammalian 293T cells using beads conjugated to anti-Flag antibody. Endogenous Bcl-x_L co-immunoprecipitated only with α- and β-subunits (Fig. 3e). The interaction with the β-subunit was blocked by the specific Bcl-x_L inhibitor ABT-737, indicating that the β-subunit binds to Bcl-x_L within the ABT-737-binding pocket (Fig. 3f).

Recombinant Bcl-x_L protein enhances the enzymatic rate of the F_1F_O ATPase

To determine whether Bcl-x_L affects the enzymatic activity of F_1F_O ATPase, the rate of ATP hydrolysis was quantified in SMVs (refs 36,37). Vesicles were treated with Triton X-100 to isolate the F_1F_O ATPase enzyme complex from the membrane. Activity of the F_1F_O ATPase was prevented by the ATP synthase inhibitor oligomycin, confirming the specificity of the reaction to the F_1F_O ATPase complex (Fig. 4a).

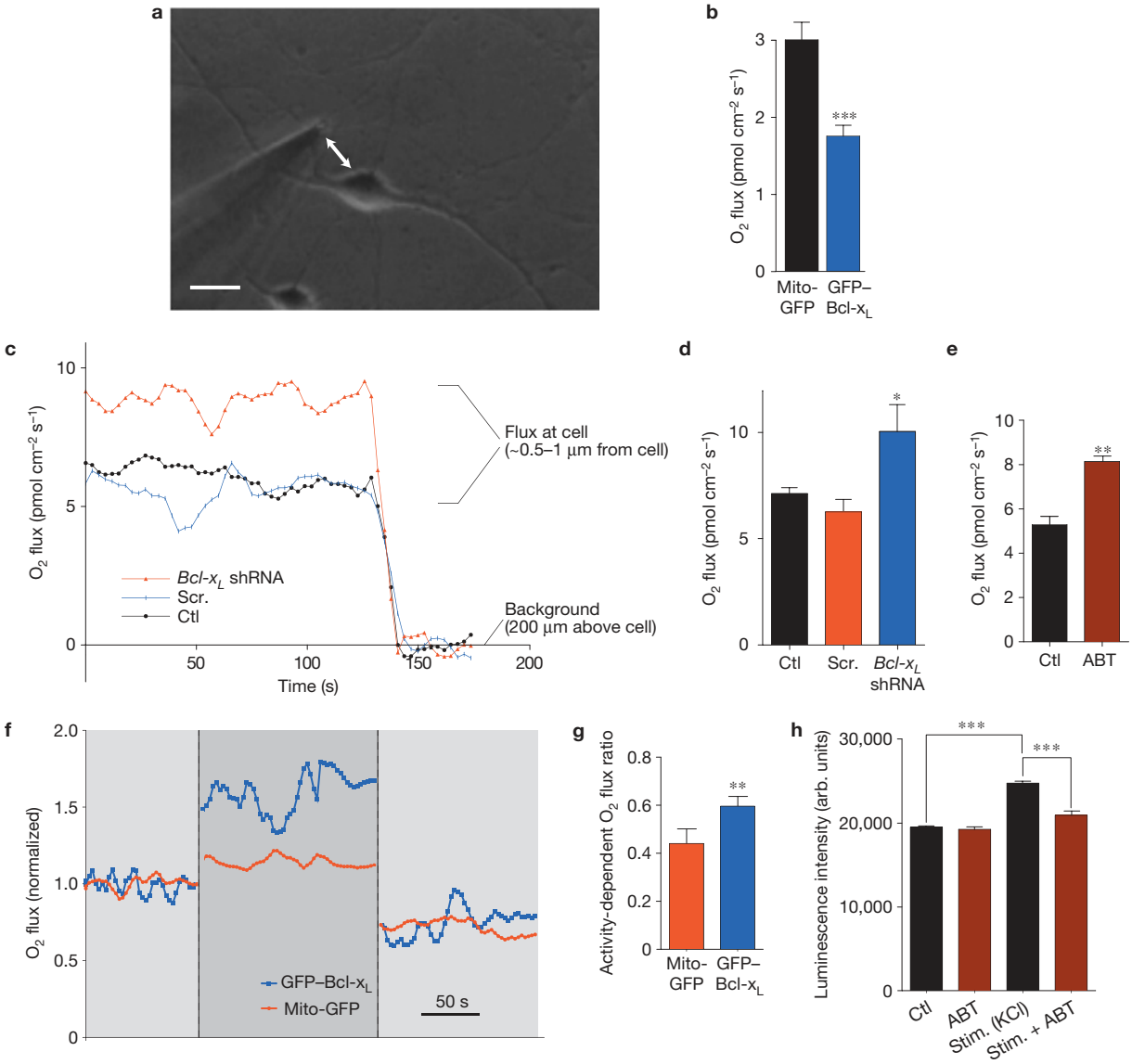

Figure 2 Bcl-x_L alters oxygen uptake by neurons. Resting Bcl-x_L-overexpressing and Bcl-x_L-depleted neurons have altered oxygen uptake. (**a**) Photomicrograph of a self-referencing amperometric O_2 microsensor positioned next to a single hippocampal neuron. Scale bar, 20 μm. (**b**) Group data for basal respiration in GFP–Bcl-x_L-expressing neurons, compared with mito-GFP-expressing neurons, at 7 days after transfection ($N = 28$ mito-GFP-expressing neurons, $N = 26$ GFP–Bcl-x_L-expressing neurons; $^{***}P < 0.0005$). The experiment was repeated in five different cultures from five different animals. (**c**) Representative traces of oxygen flux levels of single neurons. For neuronal flux measurements, a self-referencing amperometric O_2 microsensor was placed within 1 μm of the cell surface. For the background measurement, the electrode was moved 200 μm from the cell surface. Scr., scramble; Ctl, control. (**d**) Group data for basal respiration levels of single non-expressing neurons, or neurons expressing *Bcl-x_L* shRNA or scrambled shRNA at 7 days after viral transduction ($N = 10$ replicates for the control and *Bcl-x_L* shRNA, $N = 9$ replicates for scrambled shRNA; at least three independent cultures were used for studies; $^{*}P < 0.05$). (**e**) Group data for basal respiration levels of single control neurons or neurons exposed for 18 h to 10 μM ABT-737 (ABT; $N = 26$ for control and $N = 19$ for ABT-737; $^{**}P < 0.002$; at least three different cultures for each group). (**f**) Representative traces of oxygen flux levels of single neurons expressing Bcl-x_L–GFP or mito-GFP, while resting (left), stimulated with 90 mM KCl (middle) and after the addition of 5 mg ml^{-1} oligomycin (right). All values were normalized against the average oxygen flux of the same neuron at the resting flux level. (**g**) Group data for the oxygen flux of single cultured neurons expressing Bcl-x_L–GFP or mito-GFP. The leak-subtracted oxygen flux was divided by the peak oxygen flux measured during neuronal activity. Neurons were studied from four independent cultures ($N = 9$ mito-GFP control neurons, $N = 12$ GFP–Bcl-x_L-expressing neurons; $^{*}P < 0.04$). (**h**) Luminescence of firefly luciferase in cultured hippocampal neurons exposed or not to 1 μM ABT-737 for 5 min and subsequently stimulated with 90 mM KCl for 90 s ($N = 12$ wells per group; $^{***}P < 0.0001$; two different cultures for each condition). Measurement of stimulated wells was taken 5 min after washout of high K. For all panels error bars indicate s.e.m.

The addition of recombinant Bcl-x_L protein increased the rate of ATP hydrolysis (Fig. 4a) over that measured after the addition of control protein (bovine serum albumin, BSA), indicating that interaction of Bcl-x_L protein with the F_1F_O ATPase increases the enzymatic rate. Bcl-x_L protein itself had no effect on luciferase activity in the absence of SMVs (1.000 ± 0.008 versus 0.994 ± 0.006 without and with Bcl-x_L, normalized to controls, $N = 5$ wells each). In addition, the amino terminus of Bcl-x_L was not required, as recombinant Bcl-x_L

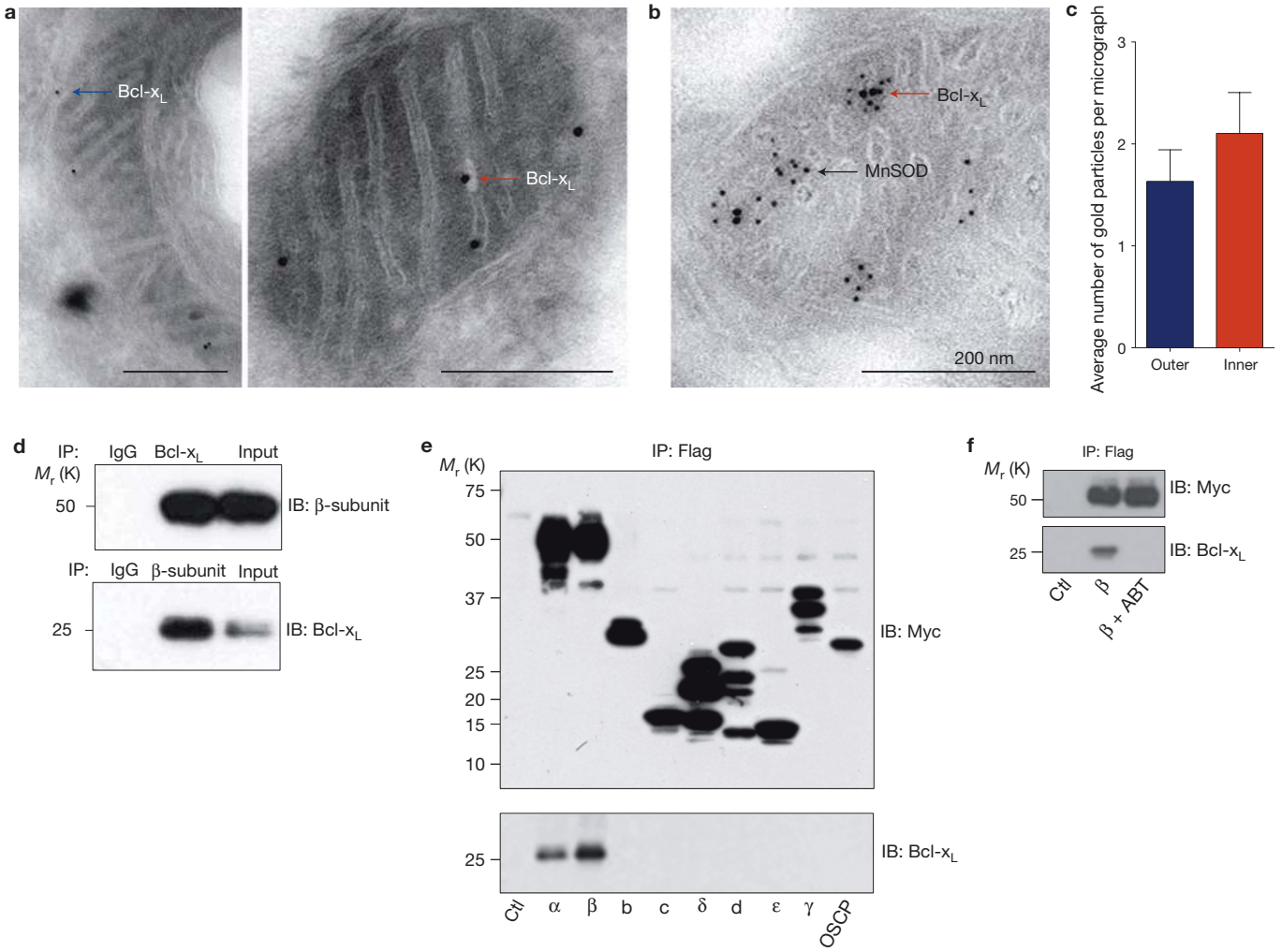

Figure 3 Bcl-x_L is expressed in the mitochondrial inner membrane and interacts with ATP synthase. (**a**) Immuno-electron micrographs from cultured neurons overexpressing Bcl-x_L at 7 days after viral transduction. Bcl-x_L immunoreactivity in the outer membrane (left, arrow) and the inner membrane cristae (right, arrow) are shown. Scale bars, 200 nm. (**b**) Immuno-electron micrographs prepared from untreated rat brain (large balls, Bcl-x_L; small balls, MnSOD). (**c**) Average number of immunogold particles per electron micrograph representing Bcl-x_L protein in the outer versus inner membrane ($N = 30$ micrographs). Error bars indicate s.e.m. (**d**) Reciprocal immunoblots (IB) of co-immunoprecipitation (IP) of Bcl-x_L and the ATP synthase β-subunit from purified rat brain ATP synthase complex. Antibodies are as indicated (immunoblot; $N = 3$). Top, the precipitating antibodies were IgG and Bcl-x_L. The right lane represents the whole-cell lysate. Bottom, the precipitating antibodies were IgG and the ATP synthase β-subunit. The right lane represents the whole-cell lysate. (**e**) Top, immunoprecipitation of the Myc–Flag-tagged ATP synthase subunits (α, β, b, c, δ, d, ε, γ, and OSCP), precipitated using the anti-Flag affinity gel and immunoblotted using anti-Myc tag antibody. Ctl, control. Bottom, western blot analysis, using anti-Bcl-x_L antibody, on the immunoprecipitated samples. (**f**) Top, immunoprecipitation of the Myc–Flag-tagged ATP synthase subunit β, precipitated using the anti-Flag affinity gel and immunoblotted using anti-Myc antibody. Cells were pre-exposed for 12 h to 1 μM ABT-737 (ABT) or vehicle. Bottom, western blot analysis, using anti-Bcl-x_L antibody on the immunoprecipitated samples. Uncropped images of blots are shown in Supplementary Fig. S8.

protein lacking the N terminus (Bcl-$x_L^{\Delta N}$) also increased the rate of ATP hydrolysis (Supplementary Fig. S5a). To determine whether endogenous Bcl-x_L contributed to the enzymatic rate, F_1F_O ATPase was exposed to ABT-737. Exposure to ABT-737 decreased the rate of ATP hydrolysis (Fig. 4b), whereas dimethylsulphoxide carrier had no effect (Supplementary Fig. S5b; $N = 3$).

The enzymatic activity of the F_1F_O ATPase was also measured in an ATP-regenerating assay where ATP concentration cannot be rate-limiting. Recombinant Bcl-x_L protein significantly enhanced the enzymatic rate of the F_1F_O ATPase; inactive Bcl-x_L protein had no effect (Fig. 4c); ABT-737 and another small-molecule inhibitor of Bcl-x_L, obatoclax[38], significantly decreased the enzymatic rate. The effect of Bcl-x_L was mimicked by the application of a recombinant truncated Bcl-x_L protein lacking the membrane-targeting region (Bcl-$x_L^{\Delta TM}$), indicating that specific membrane targeting is not necessary for this effect (Fig. 4c). These studies indicate that endogenous or exogenously applied Bcl-x_L enhances the enzymatic rate of the F_1F_O ATPase, and that the N and carboxy termini are not required for these effects. Furthermore, there was no change in the rate of ATP hydrolysis following exposure to membrane ionophores, nystatin or FCCP ($N = 3$ samples each, Supplementary Fig. S5c), indicating that the channel-producing function of Bcl-x_L is not responsible for the enhanced enzymatic rate of F_1F_O ATPase.

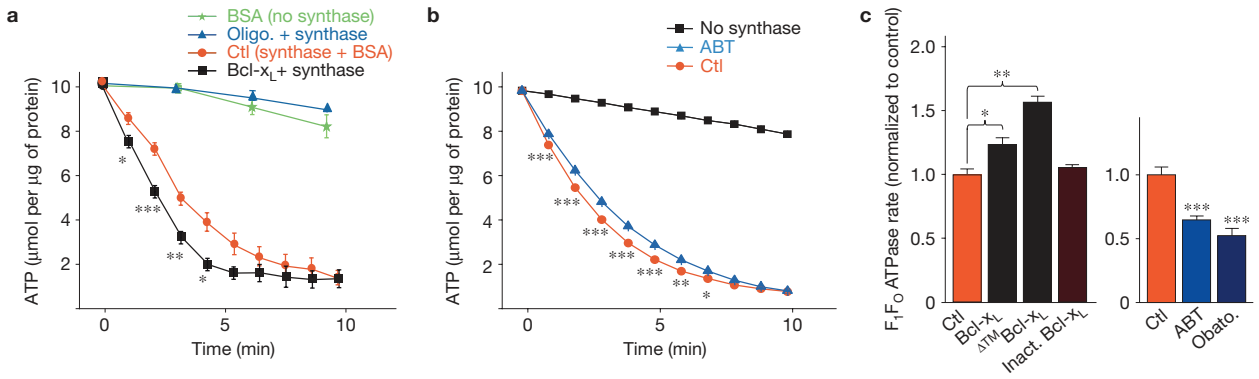

Figure 4 Bcl-x_L protein regulates ATPase activity. (**a**) Luminescence intensity of firefly luciferin–luciferase activity in the presence of ATP. $N = 3$ wells without F_1F_O ATP synthase (blank); $N = 3$ wells F_1F_O ATP synthase plus the F_O inhibitor oligomycin (Oligo.; 5 mg ml^{-1}); $N = 6$ wells synthase plus recombinant Bcl-x_L protein (0.045–0.79 mg protein per millilitre); $N = 9$ wells synthase plus control (Ctl) protein (0.05 mg ml^{-1} BSA, F_1F_O ATP synthase concentration for all experiments was 4 mg protein per millilitre). $^*P < 0.05$, $^{**}P < 0.005$, $^{***}P < 0.0005$. The experiments on Bcl-x_L versus control were repeated and confirmed on five different experimental days using at least two different F_1F_O ATPase vesicle preparations (from two different animals). (**b**) F_1F_O ATPase activity of purified F_1F_O ATP synthase in the absence and presence of ABT-737 (ABT; 20 μM). Data are shown as the percentage change in fluorescence intensity over time ($N = 3$ for each condition; $^{***}P < 0.0008$, $^{**}P < 0.003$, $^*P < 0.04$). Experiments were repeated on three independent isolations with similar results. (**c**) F_1F_O ATPase activity of the purified F_1F_O ATP synthase vesicles in the presence of the indicated recombinant proteins or reagents as a function of the rate of decrease in NADH fluorescence intensity (see Methods). Left, $N = 3$ samples in each condition; $^{**}P < 0.002$, $^*P < 0.04$; assay carried out with similar results on two independent F_1F_O ATP synthase isolations. Inact., inactive. Right, $N = 7$ samples for each condition; assay carried out with similar results on two independent isolations $^{***}P < 0.0001$. Obato., obatoclax. For all panels error bars indicate s.e.m.

Bcl-x_L inhibition attenuates H^+ sequestration into submitochondrial vesicles during F_1F_O ATPase activity

The oxygen flux studies had revealed an oligomycin-insensitive, Bcl-x_L-sensitive leak of H^+ that could contribute to an inefficiency of ATP production. To measure the H^+ leak during F_1F_O ATPase enzymatic activity, we measured the movement of H^+ ions into the SMVs in response to ATP hydrolysis. After the addition of ATP to the SMVs, ATPase activity results in a decrease in the H^+ concentration in the bath surrounding the vesicles[39] measured by a decrease in fluorescence intensity of the SMV-excluded H^+ indicator, ACMA (ref. 39; Fig. 5a). The addition of ATP to the control buffer in the absence of SMVs failed to change the ACMA fluorescence intensity (99.2 ± 1% control, $N = 6$), whereas the addition of ATP to SMVs resulted in a marked decrease in fluorescence intensity (Fig. 5b,c). Attenuation of the maximum response to ATP occurred either following inhibition of H^+ ion import through the F_O pump (oligomycin), or by leakage of H^+ out of the SMVs (FCCP). Attenuation also occurred in the presence of two different small-molecule Bcl-x_L inhibitors, ABT-737 (ref. 16) or obatoclax[38] (Fig. 5b,c), consistent with the hypothesis that inhibition of endogenous Bcl-x_L decreases the enzymatic rate or induces a H^+ leak within the SMV membrane.

Patch-clamp recordings of submitochondrial vesicles reveal a Bcl-x_L-sensitive membrane leak

To more directly measure leak conductance, we developed a method to patch clamp the SMVs isolated from native rat brain. This method was based on our previous published methods in which we patch clamped similarly sized organelles (500–1,000 nm in diameter) either within living presynaptic terminals or isolated from brain, using pipettes with diameters of ~180 nm (refs 3,40,41). In an intracellular solution lacking ATP in both the bath and pipette, a giga-ohm seal was formed on the isolated SMVs; then currents were recorded while holding the membrane at different voltages between −150 mV and +150 mV. The peak conductance was 600 pS on average. In some (Fig. 6a, left) but not all (Fig. 6c, left) recordings, gating between different levels of conductance was detected. As SMVs carry out ATP hydrolysis coupled to H^+ movement following the addition of ATP to the vesicles (see Fig. 5), and the F_1 portion of the F_1F_O ATPase faces the medium in the preparation[36], we reasoned that the addition of ATP during recordings may produce a measurable current. In contrast, however, 0.5 mM ATP consistently resulted in decreased membrane conductance of the SMVs by approximately 70% (Fig. 6a,c middle, mean data shown in second bar in Fig. 6b,d). The decrease in conductance most likely represents closure of channels and an increase in resistance caused by the effects of ATP on the membrane in series with the patched membrane.

The ATP effect indicates an ATP-responsive leak conductance associated with the F_1F_O ATPase. To determine whether the change in leak conductance occurred during ATP synthesis, succinate and ADP were added to mimic the conditions present during ATP synthesis. The decrease in membrane conductance was similar to that with ATP ($N = 3$, conductance decreased by 79 ± 8%, $P < 0.02$, paired t-test), indicating that the leak conductance was equally sensitive to ADP or ATP.

To assess the role of Bcl-x_L in determining mitochondrial membrane leak conductance, Bcl-x_L activity was inhibited pharmacologically. Both ABT-737 and obatoclax increased the conductance in the SMV membranes when added in the presence of ATP (Fig. 6a–d), although the leak was not affected by the addition of control buffer (0.1% dimethylsulphoxide, Supplementary Fig. S6a) or the addition of ABT-737 or obatoclax in the absence of ATP (Fig. 6b,d), indicating that the inhibitors themselves do not cause a leak.

To confirm the results obtained with pharmacological inhibition, knockdown of Bcl-x_L using shRNA lentiviruses was carried out on cultured hippocampal neurons. Knockdown of Bcl-x_L was confirmed with immunoblots (Fig. 6e). Consistent with the results for non-transduced controls, SMV patch-clamp recordings made from scrambled-shRNA-expressing cultures responded to ATP application

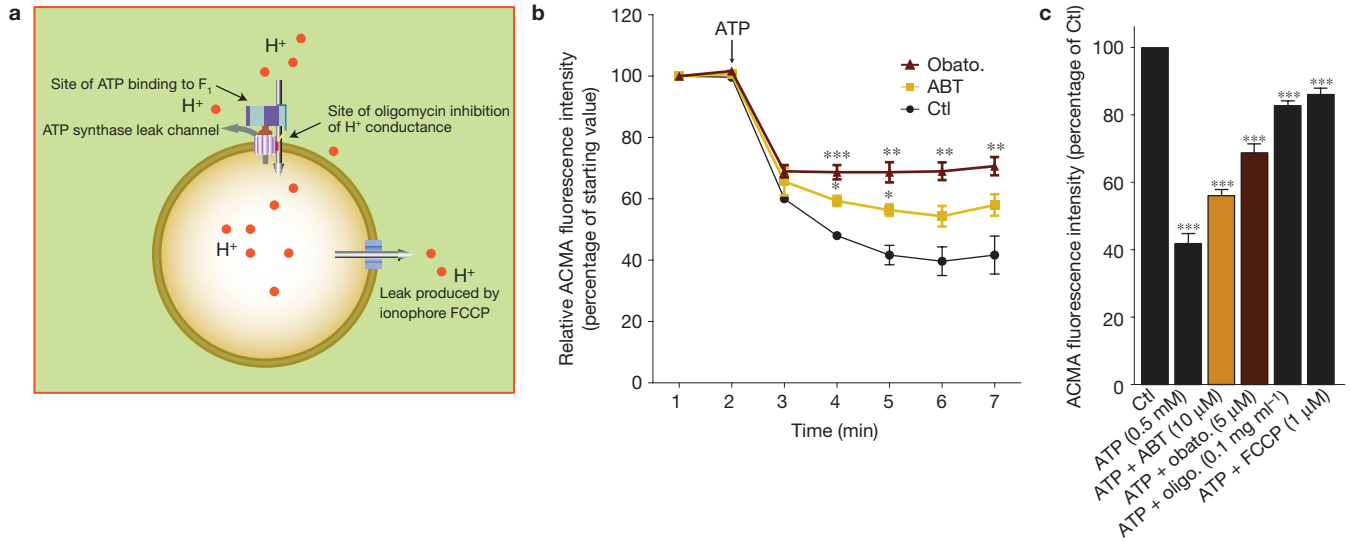

Figure 5 ATP-sensitive H^+ ion sequestration into F_1F_O ATPase vesicles (SMVs) is attenuated by Bcl-x_L inhibitors, and by oligomycin and FCCP. (**a**) Arrangement of an F_1F_O ATPase vesicle exposed to the fluorescent pH indicator, ACMA. ATP binds to F_1 to activate ATP hydrolysis and drives H^+ ions through F_O, decreasing the ACMA fluorescence intensity. Bcl-x_L inhibitors produce a H^+ leak out of the F_1F_O ATPase membrane, perhaps at the site of the F_1F_O ATPase itself, resulting in an increase in ACMA fluorescence intensity. Oligomycin blocks the movement of H^+ ions through F_O, and thus prevents a drop in the ACMA fluorescence intensity. FCCP is a H^+ ionophore that causes the leakage of H^+ out of the SMV. (**b**) Example traces of fluorescence intensity changes of the ACMA indicator over time in the presence of F_1F_O ATPase vesicles ($N = 3$ samples for each condition, repeated three times; comparing effects of reagents in the presence of ATP with the effect of ATP alone, $^*P < 0.05$; $^{**}P < 0.01$; $^{***}P < 0.0001$, one-way analysis of variance, ANOVA). Obato., obatoclax; ABT, ABT-737; Ctl, control. (**c**) Group data showing the peak effect on relative fluorescence intensity (percentage of control). The control represents the fluorescence of the ACMA indicator in the presence of SMVs before the addition of ATP ($N = 3$ samples for each group; $^*P < 0.05$; $^{***}P < 0.0001$, one-way ANOVA). Oligo., oligomycin. This study was repeated at least three times on different batches of SMVs with similar results. Error bars indicate s.e.m.

with an approximately 80% decrease in peak conductance (measured from 0 pA; Fig. 6f,g), whereas conductances from SMVs of *Bcl-x_L*-shRNA-transduced cultures had an approximately 50% decrease (Fig. 6g,h). This indicates that endogenous Bcl-x_L is required for full leak closure following ATP binding. Further studies showed that the Bcl-x_L-regulated leak conductance in SMVs is different from the oligomycin-sensitive H^+ conductance and is pharmacologically distinct from that of the ANT or K_{ATP} (Supplementary Fig. S6b–g). A non-selective proteinaceous pore that shunts H^+ ions away from H^+-translocating activities found within the membrane portion of the F_1F_O ATPase protein complex is a reasonable candidate for the ATP- and Bcl-x_L-regulated leak conductance.

Bax- and Bak-independent cell survival depends on Bcl-x_L-regulated metabolic changes

The anti-apoptotic function of Bcl-x_L can exist independently of interaction with pro-apoptotic Bcl2 family members such as Bax and Bak[42], but the mechanism of such protection is not fully understood. Glucose-free, galactose-containing media force mitochondrial metabolism. To address whether the metabolic function and the Bax- and Bak-independent survival function of Bcl-x_L overlapped, we studied the effects on ATP levels and cell survival of overexpression of Bcl-x_L in Bax, Bak double-knockout (DKO) mouse embryonic fibroblasts (MEFs). ATP levels increased over time in Bcl-x_L-expressing cells on galactose medium (Supplementary Fig. S7a). The change in the medium decreased the level of survival of the MEFs; Bcl-x_L overexpression enhanced the level of survival, indicating that increased mitochondrial ATP production by Bcl-x_L may rescue cells from metabolic compromise in the absence of Bax or Bak (Supplementary Fig. S7b).

DISCUSSION

Previous studies show that Bcl-x_L increases mitochondrial biomass[9,10]. Therefore, it was surprising to find that resting neurons expressing Bcl-x_L use less oxygen but have higher ATP levels and decreased glycolysis levels. Stimulated Bcl-x_L-expressing neurons use more of the total oxygen uptake for ATP production than stimulated controls. Moreover, Bcl-x_L acutely increases the level of ATP production during neuronal stimulation, because ABT-737 completely prevents such an increase. These findings indicate that neuronal activity induces Bcl-x_L-dependent changes in mitochondrial metabolism. In stimulated neurons, Bcl-x_L expressed on endoplasmic reticulum membranes may influence the directed release of endoplasmic reticulum calcium towards mitochondrial calcium uptake mechanisms that may further enhance ATP synthesis[43].

Our evidence supports a Bcl-x_L- and ATP-modulated H^+ leak in the inner mitochondrial membrane that decreases efficiency. An ATP-sensitive leak of H^+ measured with the H^+ indicator ACMA is re-activated by pharmacological inhibitors of Bcl-x_L activity; patch-clamp recordings of SMVs reveal a large ion conductance attenuated by ATP, and re-activated by pharmacological inhibition of Bcl-x_L activity or suppression of Bcl-x_L expression. The leaky membrane of control SMVs may result from preparation of the vesicles without adenine nucleotides, but an adenine-nucleotide-deficient state may also exist under pathophysiological conditions such as ischaemia or neurodegenerative disorders. Re-introducing ATP or ADP rapidly closes the leak, indicating that ATP- or ADP-induced leak closure is an integral aspect of enzymatic function.

Although increased ATP synthase enzymatic activity will not directly increase efficiency, recombinant Bcl-x_L protein and the Bcl-x_L inhibitors regulate the enzymatic rate as measured by two assays

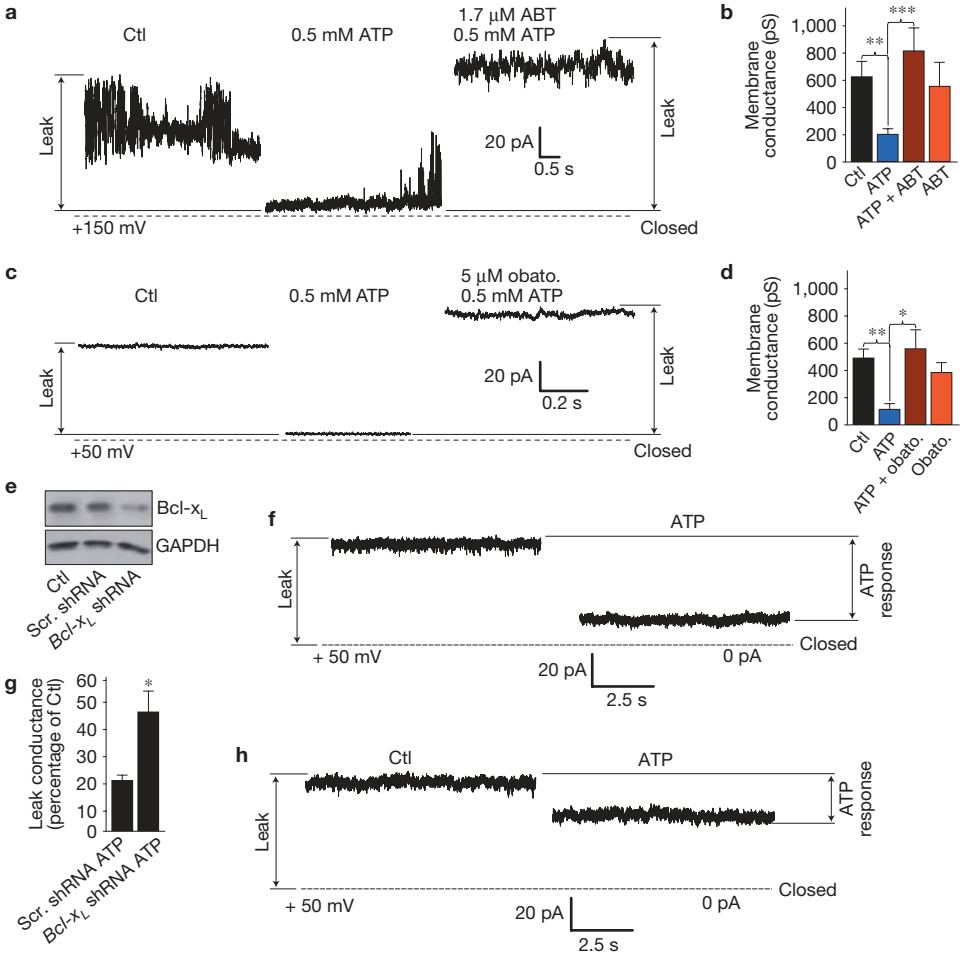

Figure 6 Pharmacological inhibition or depletion of Bcl-x_L reverses leak closure in patch-clamp recordings of isolated ATP F_1F_O ATPase vesicles. (**a**) Example SMV patch-clamp recording at the indicated voltage before and after ATP and ATP + ABT-737 exposure. The dashed line represents 0 pA. Ctl, control; ABT, ABT-737. (**b**) Group data of membrane conductances of all recordings such as shown in **a** (SMV recordings from left to right, $N = 30, 23, 19, 7$; $^{**}P < 0.002$, $^{***}P < 0.0009$). The last bar shows experiments in which the Bcl-x_L inhibitor was added to patches in the absence of ATP. (**c**) Example SMV patch-clamp recording at the indicated voltage before and after ATP and ATP plus obatoclax (Obato.) exposure. The dashed line represents 0 pA. (**d**) Group data of membrane conductances of all recordings such as shown in **c** (SMV recordings from left to right, $N = 23, 9, 15, 14$; $^{**}P < 0.004$, $^{*}P < 0.04$). The last bar shows experiments in which the Bcl-x_L inhibitor was added to patches in the absence of ATP. (**e**) Western blot for endogenous Bcl-x_L protein. Cell lysates prepared from non-transduced control hippocampal neuron cultures, scrambled-shRNA-expressing neuron cultures and *Bcl-x_L*-shRNA-expressing neuron cultures at 4 days after transduction. The protein concentration was controlled by immunoblotting for GAPDH. (**f**) SMV patch-clamp recordings before and after the addition of 0.5 mM ATP. SMVs were prepared from hippocampal neurons expressing control (scrambled) shRNA at 4 days after transduction. (**g**) Group data from all recordings of control (scrambled, Scr.) shRNA or *Bcl-x_L* shRNA. Shown is the membrane leak conductance remaining after the addition of ATP as a percentage of the initial conductance before the addition of ATP ($N = 5$ control recordings, $N = 7$ *Bcl-x_L*-shRNA recordings; $^{*}P < 0.03$). (**h**) SMV patch-clamp recordings before and after the addition of ATP. SMVs were prepared from hippocampal neurons expressing *Bcl-x_L* shRNA at 4 days after transduction. For all panels error bars indicate s.e.m. Uncropped images of blots are shown in Supplementary Fig. S8.

(Fig. 4). These results raise the possibility that a change in position of certain proteins within the F_1F_O ATPase complex regulates enzymatic rate and leak closure.

Bcl-x_L has been found to act at the outer membrane[26–29]. How Bcl-x_L targets to the inner membrane is not known. Reports have located the related protein Bcl2 or Bcl-x_L to the inner membrane[30,44] in the same compartment as the β-subunit of the ATP synthase[31] (Chen and Hardwick, unpublished data), and have indicated that Bax requires the F_1F_O ATPase to initiate apoptosis[45], and that oligomycin suppresses apoptosis[46]. The present study confirms and extends these findings, localizing Bcl-x_L to the β-subunit by immuno-electron microscopy, by co-immunoprecipitation with the F_1F_O ATPase and by co-immunoprecipitation with purified mammalian α- and β-subunits. Binding of Bcl-x_L to the β-subunit is reversed by ABT-737, indicating that the ABT-737-binding region is needed for binding to the β-subunit. Consistent with this, mutant recombinant Bcl-x_L proteins lacking the BH4 domain (N terminus) or the membrane-targeting domain (C terminus) act as effectively as the full-length protein to increase the rate of ATP hydrolysis.

The protein responsible for the leak channel itself is as yet unidentified. Only a few of the proteins associated with F_1F_O ATPase have been characterized[37,47]. Other ATP-sensitive candidate channels of the inner membrane include the ANT, mito-K_{ATP} and members of the UCP family[20,48–52]. Although upregulation of UCP activity in brain enhances

neuroprotection, levels of homologues of the UCPs in healthy brain are relatively low[53–55]. It is therefore likely that we have encountered a previously undescribed conductance within the F_1F_O ATPase.

The increase in ATP production by Bcl-x_L-overexpressing healthy neurons was anticipated by studies showing an increase in the release of ATP and phosphocreatine in Bcl-x_L-overexpressing non-neuronal cells undergoing death[7,56]. Protection from cell death was attributed to enhanced release of ATP from mitochondria through Bcl-x_L-regulated VDAC opening in the outer membrane. Our results do not preclude Bcl-x_L activity in the outer membrane. In fact, it is likely that enhanced ATP production by the inner membrane F_1F_O ATP synthase complex requires the maintenance of VDAC in an open configuration to release the newly synthesized ATP into the cytosol.

Enhanced metabolic efficiency by Bcl-x_L in neurons may produce resistance to death of tumour cells[57,58], and enhancement of cell survival shown here is independent of Bax and Bak (Supplementary Fig. S7). Some tumour cells manifest metabolic changes attributed to an increase in the level of aerobic glycolysis[59–61]. We show that healthy neurons use Bcl-x_L to produce a different kind of metabolic efficiency. Nevertheless, the changes in metabolism produced by Bcl-x_L may enhance resistance to pathological stressors including hypoxia and substrate deprivation and may maintain cytosolic ATP levels in the face of the increased energy demand provided by synaptic development, and long- or short-term changes in synaptic plasticity. □

METHODS

Methods and any associated references are available in the online version of the paper at http://www.nature.com/naturecellbiology

Note: Supplementary Information is available on the Nature Cell Biology website

ACKNOWLEDGEMENTS

We thank L. K. Kaczmarek for scientific discussion and review of the manuscript. We thank C. Kinnally and N. Danial for the gift of Bax, Bak (DKO) MEFs and Institut de Recherches Servier, Croissy sur Seine, France for ABT-737. This work was supported by NIH NS064967 (E.A.J.) and NS37402 (J.M.H.).

AUTHOR CONTRIBUTIONS

K.N.A. and E.A.J. conceived the project, carried out most of the experiments, analysed the data and prepared the manuscript. H.L. and L.C. contributed experiments to Figs 1 and 2. L.B. contributed experiments to Fig. 6. L.Z., S.S. and M.A.M. contributed to Fig. 4. E.L. and P.N. contributed to Fig. 3. B.F. helped with Fig. 6. M.G. and C.R. contributed experiments to Fig. 3 and Supplementary Fig. S2. S.M.M. and E.M. contributed to Fig. 1. Y.C. and G.C.S. contributed to discussion. P.J.S.S. provided experimental design and discussion for Figs 1 and 2. J.M.H. designed Bcl-x_L immunolocalization experiments, and contributed intellectually as well as in manuscript preparation.

COMPETING FINANCIAL INTERESTS

G.C. Shore is a shareholder in Gemin X Pharmaceuticals Inc.

Published online at http://www.nature.com/naturecellbiology
Reprints and permissions information is available online at http://www.nature.com/reprints

1. Banasiak, K. J., Xia, Y. & Haddad, G. G. Mechanisms underlying hypoxia-induced neuronal apoptosis. *Prog. Neurobiol.* **62,** 215–249 (2000).
2. Youle, R. J. & Strasser, A. The BCL-2 protein family: opposing activities that mediate cell death. *Nat. Rev. Mol. Cell Biol.* **9,** 47–59 (2008).
3. Fannjiang, Y. *et al.* BAK alters neuronal excitability and can switch from anti- to pro-death function during postnatal development. *Dev. Cell* **4,** 575–585 (2003).
4. Kim, H. *et al.* Hierarchical regulation of mitochondrion-dependent apoptosis by BCL-2 subfamilies. *Nat. Cell Biol.* **8,** 1348–1358 (2006).
5. Wang, C. & Youle, R. J. The role of mitochondria in apoptosis. *Annu. Rev. Genet* **43,** 95–118 (2009).
6. Hardwick, J. M. & Youle, R. J. SnapShot: BCL-2 proteins. *Cell* **138,** 404.e1–404.e2 (2009).
7. Gottlieb, E., Armour, S. M. & Thompson, C. B. Mitochondrial respiratory control is lost during growth factor deprivation. *Proc. Natl Acad. Sci. USA* **99,** 12801–12806 (2002).
8. Krajewska, M. *et al.* Dynamics of expression of apoptosis-regulatory proteins Bid, Bcl-2, Bcl-X, Bax and Bak during development of murine nervous system. *Cell Death Differ.* **9,** 145–157 (2002).
9. Li, H. *et al.* Bcl-xL induces Drp1-dependent synapse formation in cultured hippocampal neurons. *Proc. Natl Acad. Sci. USA* **105,** 2169–2174 (2008).
10. Berman, S. B. *et al.* Bcl-x L increases mitochondrial fission, fusion, and biomass in neurons. *J. Cell Biol.* **184,** 707–719 (2009).
11. Mozhayeva, M. G., Sara, Y., Liu, X. & Kavalali, E. T. Development of vesicle pools during maturation of hippocampal synapses. *J. Neurosci.* **22,** 654–665 (2002).
12. Verstreken, P. *et al.* Synaptic mitochondria are critical for mobilization of reserve pool vesicles at *Drosophila* neuromuscular junctions. *Neuron* **47,** 365–378 (2005).
13. Li, Z., Okamoto, K., Hayashi, Y. & Sheng, M. The importance of dendritic mitochondria in the morphogenesis and plasticity of spines and synapses. *Cell* **119,** 873–887 (2004).
14. Hickman, J. A., Hardwick, J. M., Kaczmarek, L. K. & Jonas, E. A. Bcl-xL inhibitor ABT-737 reveals a dual role for Bcl-xL in synaptic transmission. *J. Neurophysiol.* **99,** 1515–1522 (2008).
15. Manfredi, G., Yang, L., Gajewski, C. D. & Mattiazzi, M. Measurements of ATP in mammalian cells. *Methods (Duluth)* **26,** 317–326 (2002).
16. Oltersdorf, T. *et al.* An inhibitor of Bcl-2 family proteins induces regression of solid tumours. *Nature* **435,** 677–681 (2005).
17. Land, S. C., Porterfield, D. M., Sanger, R. H. & Smith, P. J. The self-referencing oxygen-selective microelectrode: detection of transmembrane oxygen flux from single cells. *J. Exp. Biol.* **202,** 211–218 (1999).
18. Brand, M. D. The efficiency and plasticity of mitochondrial energy transduction. *Biochem. Soc. Trans.* **33,** 897–904 (2005).
19. Harper, M. E., Bevilacqua, L., Hagopian, K., Weindruch, R. & Ramsey, J. J. Ageing, oxidative stress, and mitochondrial uncoupling. *Acta Physiol. Scand.* **182,** 321–331 (2004).
20. Andrews, Z. B., Diano, S. & Horvath, T. L. Mitochondrial uncoupling proteins in the CNS: in support of function and survival. *Nat. Rev. Neurosci.* **6,** 829–840 (2005).
21. Kunjilwar, K. K., Fishman, H. M., Englot, D. J., O'Neil, R. G. & Walters, E. T. Long-lasting hyperexcitability induced by depolarization in the absence of detectable Ca^{2+} signals. *J. Neurophysiol.* **101,** 1351–1360 (2009).
22. Bouvier, D. *et al.* EphA4 is localized in clathrin-coated and synaptic vesicles in adult mouse brain. *J. Neurochem.* **113,** 153–165 (2010).
23. Rolfe, D. F. & Brown, G. C. Cellular energy utilization and molecular origin of standard metabolic rate in mammals. *Physiol. Rev.* **77,** 731–758 (1997).
24. Hackenbrock, C. R., Rehn, T. G., Weinbach, E. C. & Lemasters, J. J. Oxidative phosphorylation and ultrastructural transformation in mitochondria in the intact ascites tumor cell. *J. Cell Biol.* **51,** 123–137 (1971).
25. Vander Heiden, M. G. *et al.* Bcl-xL promotes the open configuration of the voltage-dependent anion channel and metabolite passage through the outer mitochondrial membrane. *J. Biol. Chem.* **276,** 19414–19419 (2001).
26. Lovell, J. F. *et al.* Membrane binding by tBid initiates an ordered series of events culminating in membrane permeabilization by Bax. *Cell* **135,** 1074–1084 (2008).
27. Galonek, H. L. & Hardwick, J. M. Upgrading the BCL-2 network. *Nat. Cell Biol.* **8,** 1317–1319 (2006).
28. Boise, L. H. *et al.* Bcl-x, a bcl-2-related gene that functions as a dominant regulator of apoptotic cell death. *Cell* **74,** 597–608 (1993).
29. Kaufmann, T. *et al.* Characterization of the signal that directs Bcl-x(L), but not Bcl-2, to the mitochondrial outer membrane. *J. Cell Biol.* **160,** 53–64 (2003).
30. Hockenbery, D., Nunez, G., Milliman, C., Schreiber, R. D. & Korsmeyer, S. J. Bcl-2 is an inner mitochondrial membrane protein that blocks programmed cell death. *Nature* **348,** 334–336 (1990).
31. Gotow, T. *et al.* Selective localization of Bcl-2 to the inner mitochondrial and smooth endoplasmic reticulum membranes in mammalian cells. *Cell Death Differ.* **7,** 666–674 (2000).
32. Kobayashi, T. *et al.* Ultrastructural localization of superoxide dismutase in human skin. *Acta Derm. Venereol.* **73,** 41–45 (1993).
33. Suzuki, K. *et al.* Manganese-superoxide dismutase in endothelial cells: localization and mechanism of induction. *Am. J. Physiol.* **265,** H1173–H1178 (1993).
34. Akai, F. *et al.* Immunocytochemical localization of manganese superoxide dismutase (Mn-SOD) in the hippocampus of the rat. *Neurosci. Lett.* **115,** 19–23 (1990).
35. Belzacq, A. S. *et al.* Bcl-2 and Bax modulate adenine nucleotide translocase activity. *Cancer Res.* **63,** 541–546 (2003).
36. Chan, T. L., Greenawalt, J. W. & Pedersen, P. L. Biochemical and ultrastructural properties of a mitochondrial inner membrane fraction deficient in outer membrane and matrix activities. *J. Cell Biol.* **45,** 291–305 (1970).
37. Ko, Y. H., Delannoy, M., Hullihen, J., Chiu, W. & Pedersen, P. L. Mitochondrial ATP synthasome. Cristae-enriched membranes and a multiwell detergent screening assay yield dispersed single complexes containing the ATP synthase and carriers for Pi and ADP/ATP. *J. Biol. Chem.* **278,** 12305–12309 (2003).
38. Nguyen, M. *et al.* Small molecule obatoclax (GX15-070) antagonizes MCL-1 and overcomes MCL-1-mediated resistance to apoptosis. *Proc. Natl Acad. Sci. USA* **104,** 19512–19517 (2007).

39. Caviston, T. L., Ketchum, C. J., Sorgen, P. L., Nakamoto, R. K. & Cain, B. D. Identification of an uncoupling mutation affecting the b subunit of F1F0 ATP synthase in *Escherichia coli*. *FEBS Lett.* **429,** 201–206 (1998).
40. Bonanni, L. *et al*. Zinc-dependent multi-conductance channel activity in mitochondria isolated from ischemic brain. *J. Neurosci.* **26,** 6851–6862 (2006).
41. Jonas, E. A., Buchanan, J. & Kaczmarek, L. K. Prolonged activation of mitochondrial conductances during synaptic transmission. *Science* **286,** 1347–1350 (1999).
42. Cheng, E. H., Levine, B., Boise, L. H., Thompson, C. B. & Hardwick, J. M. Bax-independent inhibition of apoptosis by Bcl-XL. *Nature* **379,** 554–556 (1996).
43. Rizzuto, R. *et al*. Ca^{2+} transfer from the ER to mitochondria: when, how and why. *Biochim. Biophys. Acta* **1787,** 1342–1351 (2009).
44. Kluck, R. M., Bossy-Wetzel, E., Green, D. R. & Newmeyer, D. D. The release of cytochrome c from mitochondria: a primary site for Bcl-2 regulation of apoptosis. *Science* **275,** 1132–1136 (1997).
45. Matsuyama, S., Xu, Q., Velours, J. & Reed, J. C. The mitochondrial F0F1-ATPase proton pump is required for function of the proapoptotic protein Bax in yeast and mammalian cells. *Mol. Cell.* **1,** 327–336 (1998).
46. Shchepina, L. A. *et al*. Oligomycin, inhibitor of the F0 part of H+-ATP-synthase, suppresses the TNF-induced apoptosis. *Oncogene* **21,** 8149–8157 (2002).
47. Chen, C. *et al*. Mitochondrial ATP synthasome: three-dimensional structure by electron microscopy of the ATP synthase in complex formation with carriers for Pi and ADP/ATP. *J. Biol. Chem.* **279,** 31761–31768 (2004).
48. O'Rourke, B. Evidence for mitochondrial K^+ channels and their role in cardioprotection. *Circul. Res.* **94,** 420–432 (2004).
49. Crompton, M. The mitochondrial permeability transition pore and its role in cell death. *Biochem. J.* **341,** 233–249 (1999).
50. Costa, A. D. & Garlid, K. D. MitoKATP activity in healthy and ischemic hearts. *J. Bioenerg. Biomembr.* **41,** 123–126 (2009).
51. Liu, T. & O'Rourke, B. Regulation of mitochondrial Ca^{2+} and its effects on energetics and redox balance in normal and failing heart. *J. Bioenerg. Biomembr.* **41,** 127–132 (2009).
52. Porter, R. K. Uncoupling protein 1: a short-circuit in the chemiosmotic process. *J. Bioenerg. Biomembr.* **40,** 457–461 (2008).
53. Diano, S. *et al*. Uncoupling protein 2 prevents neuronal death including that occurring during seizures: a mechanism for preconditioning. *Endocrinology* **144,** 5014–5021 (2003).
54. Horvath, T. L., Diano, S. & Barnstable, C. Mitochondrial uncoupling protein 2 in the central nervous system: neuromodulator and neuroprotector. *Biochem. Pharmacol.* **65,** 1917–1921 (2003).
55. Sullivan, P. G., Springer, J. E., Hall, E. D. & Scheff, S. W. Mitochondrial uncoupling as a therapeutic target following neuronal injury. *J. Bioenerg. Biomembr.* **36,** 353–356 (2004).
56. Vander Heiden, M. G. *et al*. Outer mitochondrial membrane permeability can regulate coupled respiration and cell survival. *Proc. Natl Acad. Sci. USA* **97,** 4666–4671 (2000).
57. Chonghaile, T. N. & Letai, A. Mimicking the BH3 domain to kill cancer cells. *Oncogene* **27** (suppl. 1), S149–S157 (2008).
58. Vander Heiden, M. G., Cantley, L. C. & Thompson, C. B. Understanding the Warburg effect: the metabolic requirements of cell proliferation. *Science* **324,** 1029–1033 (2009).
59. Frezza, C. & Gottlieb, E. Mitochondria in cancer: not just innocent bystanders. *Semin. Cancer Biol.* **19,** 4–11 (2009).
60. Warburg, O. On respiratory impairment in cancer cells. *Science* **124,** 269–270 (1956).
61. Golshani-Hebroni, S. G. & Bessman, S. P. Hexokinase binding to mitochondria: a basis for proliferative energy metabolism. *J. Bioenerg. Biomembr.* **29,** 331–338 (1997).

DOI: 10.1038/ncb2330

METHODS

Primary cultures of rat hippocampal neurons and transfections. Primary rat hippocampal neurons were prepared as described previously[62,63] and were transfected with 2.5 M calcium phosphate at DIV5 (5 days *in vitro*) with an efficiency of ~1–5%. Neurons were transduced with a lentiviral construct at DIV4–8 and studied at DIV10–14 with an efficiency of near 100%.

Viral constructs. Lentiviruses expressing Bcl-x_L with an N-terminal GFP tag were used to transduce cultured hippocampal neurons, achieving almost 100% efficiency. Expression of GFP–Bcl-x_L facilitates determination of protein levels by western blotting with an anti-GFP antibody (Anti-GFP Product #06-896 Upstate, 1:500). Full-length GFP–Bcl-x_L was subcloned into a lentiviral vector c-FUW (ref. 64). Viral constructs were packaged in 293T cells by co-transfection with packaging plasmid δ8.9 and envelope plasmid VSVG.48, and at 60 h after transfection, virus-containing supernatant was collected and used to transduce cultured hippocampal neurons. Transduced neurons were studied at ~7 days after transduction.

Lentiviral shRNA knockdown of Bcl-x_L. The lentiviral plasmids expressing shRNAs were from Open Biosystems. The hairpin sequence against rat *Bcl-x_L* was: 5′-CGGGCTCACTCTTCAGTCGGAATAGTGAAGCCACAGATGTATTCCGACT-GAAGAGTGAGCCCA-3′.

For a control, the scrambled, non-silencing shRNA sequence (Open Biosystems, catalogue number RHS4346) was used. Viruses were produced according to published methods[65]. The pGIPZ vector, containing either an shRNA sequence against *Bcl-x_L* or the scrambled sequence was co-transfected with the packaging Δ8.9 and the vesicular stomatitis virus G protein vectors into HEK293T cells. The supernatant was purified after 72 h and added to the hippocampal cultures. The isolation of ATP F_1F_O ATPases was carried out 4 days after viral transduction of the neurons.

Luciferase assay for *in vitro* ATP and ADP measurements. Cellular ATP levels were measured following acute cell membrane lysis in a plate reader (Perkin–Elmer) in the presence of luciferin–luciferase (ApoSENSOR, Biovision). Luminescence values were normalized to protein concentration for each well (carried out using the Pierce BSA method).

Cytosolic ATP-luminescence intensity measured *in situ*. To continually monitor cytosolic ATP in intact cells, hippocampal neurons (E19, embryonic day 19) were transduced with a luciferase (firefly) lentiviral vector on DIV-4. The CSCW2–Luc–IRES–eGFP vectors were co-transfected into 293T cells with lentiviral packaging genome and envelope. Approximately 10^6 viral particles were used per 14 mm coverslip containing between 10^4 and 10^5 cells. Neurons were also co-transfected with plasmid DNA for either mito-GFP (control) or BCLxL–eGFP (efficiency of >50%) using magnetofection[66] (NeuroMag; OZ Biosciences)[9]. After 4–7 days of incubation, neurobasal growth media (Invitrogen) was replaced with warm ACSF (artificial cerebrospinal fluid) containing 120 mM NaCl, 3.1 mM KCl, 0.4 mM KH_2PO_4, 20 mM HEPES (pH 7.4), 5 mM $NaHCO_3$, 1.2 mM $NaSO_4$, 1.3 mM $CaCl_2$, 5.5 mM glucose and 1 mM D-luciferin (Na salt; BD BioSciences). Light output from neurons was assessed in a custom-built, heated (37°) luminometer that includes a computer-controlled UNIBLITZ high-speed electronic shutter (Vincent Associates) and a photo-multiplier tube (R464; Hamamatsu Photonics). A concentration of 0.5 mM luciferin or greater generated maximum light output for a given coverslip. Once steady-state light output had been reached, mitochondrial ATP production was inhibited with oligomycin (10 mg ml^{-1}). After 15 min, ATP-dependent light levels were normalized for ATP by permeabilizing the neurons with a mock intracellular buffer[67]. Luciferase expression in neurons was verified by imaging single neurons for light output with a high-intensity CCD (charge-coupled device; C5405-50; Hamamatsu Photonics) mounted on an inverted microscope (Axiovert 135 TV; Carl Zeiss). A ×40 oil-immersion objective with a high numerical aperture (Fluar; Carl Zeiss) was used to ensure efficient light capture. Photons were integrated using custom-built acquisition software (BioCurrents Research Center).

Oxygen flux measurements. Oxygen uptake was measured in single neurons in culture using a sensitive oxygen electrode[17]. Oxygen flux was recorded using a 2–4 μm-diameter electrode at 5 μm from the cell that was moved with a displacement of 10 μm in the X–Y axes so that the oxygen-sensing electrode was positioned repeatedly closer to and farther from the cell. The current detected at two positions results in a differential current that can be translated into oxygen flux given the known oxygen concentration in the bath and the distance of the excursion of the electrode between the two points[17] (Supplementary Fig. S3a,b). The measured current associated with oxygen flux across the neuronal membrane was lower after treatment with oligomycin (Supplementary Fig. S3b). The measured current was further lowered by treatment of cells with the electron transport inhibitor antimycin A (Supplementary Fig. S3b). For oxygen flux measurements carried out during neuronal activity, cells were perfused with an osmotically balanced extracellular solution containing a high KCl concentration (90 mM KCl, 64 mM NaCl, 2 mM $MgCl_2$, 10 mM glucose, 10 mM HEPES, 2 mM $CaCl_2$; pH 7.4, 300 mOsm) for one minute followed by cessation of perfusion for one minute during which peak oxygen flux was measured. Cells were again perfused with normal extracellular buffer (KCl lowered to 2.5 mM) for one minute, followed by the addition of oligomycin (20 mg ml^{-1}) to the bath. Oxygen flux was measured after cessation of perfusion and reaching a stable value for at least 5 min.

F_1F_O ATPase vesicle preparation. Rodent whole brain without cerebellum was minced in isolation buffer (250 mM sucrose, 20 mM HEPES, at pH 7.2, 1 mM EDTA and BSA 0.5%). Tissue was homogenized in a Dounce homogenizer, then centrifuged at low speed (1300rcf-set tabletop to 4,000) to pellet nuclear material. Supernatant was centrifuged at high speed (13,000rcf) to pellet mitochondria and synaptosomes. Synaptosomes were disrupted with a nitrogen decompression chamber (Parr Instruments) at 1,200 psi for 10 min, followed by rapid decompression. Mitochondrial and burst synaptosomes were layered onto Ficoll gradients (10% and 7.5% Ficoll) and centrifuged in a Beckman ultracentrifuge at 32,500 rpm for 20 min. The pellet was washed and resuspended in isolation buffer (approximately 4–10 mg ml^{-1} protein), combined with an equal volume of digitonin (1% = 10 mg ml^{-1} isobuffer), incubated on ice for 15 min and centrifuged twice at 9,000g for 10 min. The pellet was resuspended in 200 μl of isolation buffer, and 2 μl of 10% Lubrol PX (C12E9; Calbiochem) was added, mixed and allowed to sit on ice for 15 min. The Lubrol–mitochondria mixture was layered onto isolation buffer and centrifuged at 39,000 rpm for 1 h. The final pellet was washed in isolation buffer and centrifuged at 13,000 rpm.

Luciferase assay on F_1F_O ATPase. ATP hydrolysis was measured using the BioVision Aposensor ATP Assay Kit, according to the manufacturer's protocol in the presence of 30–40 μg F_1F_O ATPase and 0.5 mM ATP. In some experiments, 10 μLBcl-x_L (0.045–0.79 mg ml^{-1}), 5 μg ml^{-1} oligomycin, 1 μM FCCP, nystatin (450 mg ml^{-1}), 17 μM ABT-737 or 0.1% dimethylsulphoxide was added to the mixture. Data are displayed as millimoles of ATP hydrolysis per minute per milligram SMV protein. All experiments used three wells for each condition, and the experiments were repeated at least three times for each condition on samples from different F_1F_O ATPase isolations.

ATP synthase enzyme activity assay. The ATPase activity was measured using the assay kit from Mitosciences (catalogue number MS541), according to the manufacturer's protocol and published methods[68]. Briefly, 5 mg F_1F_O ATPase (per well) was detergent-extracted and immunocaptured overnight within the 96-well plates. Inhibitors of Bcl-x_L were added to the immobilized enzyme and incubated for 20 min before the addition of the reagent mix and measurement. The oxidation of NADH to NAD^+ results from a coupled reaction catalysed by pyruvate kinase and lactate dehydrogenase in the presence of phosphoenolpyruvate, which is dependent on ADP production by the ATPase in the presence of ATP. The change in fluorescence intensity as NADH is oxidized was measured as a decrease in absorbance at 340 nm using a PerkinElmer VICTOR3 multilabel plate reader.

Electrophysiology. F_1F_O ATPase vesicle recordings were made by forming a giga-ohm seal onto F_1F_O ATPase vesicles in intracellular solution (120 mM KCl, 8 mM NaCl, 0.5 mM EGTA and 10 mM HEPES, at pH 7.3) using an Axopatch 200B amplifier (Axon Instruments) at room temperature (22–25 °C). Recording electrodes were pulled from borosilicate glass capillaries (WPI) with a final resistance in the range of 80–120 MW. SMVs were visualized by phase-contrast microscopy with a Nikon or Zeiss inverted microscope. Signals were filtered at 5 kHz using the amplifier circuitry. Data were analysed using pClamp 10.0 software (Axon Instruments). All population data were expressed as mean ± s.e.m.. Membrane currents under different experimental conditions were assessed by measuring the peak membrane current (in pico-amperes)—the baseline current. The baseline current was defined as a nonspecific electrode leak current. All current measurements were adjusted for the holding voltage assuming a linear current–voltage relationship: the resulting conductances are expressed in picosiemens according to the equation $G = V/\Delta I$, where G is the conductance in picosiemens, V is the membrane holding voltage in millivolts and ΔI is the peak membrane current in pico-amperes − baseline current in pico-amperes. Group data were quantified in terms of conductance.

ATP-driven quenching of ACMA. ACMA (9-amino-6-chloro-2-methoxyacridine) fluorescence quenching was measured according to previously published methods[69]. ACMA (2 μM; Sigma-Aldrich) was added to 5 μg isolated F_1F_O ATPase vesicles[47], in the presence of ATP (1 mM), inhibitors of Bcl-x_L, oligomycin or FCCP at concentrations described in the text (total volume of 100 μl). F_1F_O ATPase vesicle suspensions were excited at 410 nm, and emission was measured at 490 nm, using a PerkinElmer VICTOR3 multilabel plate reader.

Electron microscopy. Hippocampal neuron cultures (DIV13–14) prepared from E18 embryonic rats were transduced with lentiviruses expressing GFP or GFP–Bcl-x_L fusion protein to achieve gene expression in approximately 100% of the neurons[9], and at 7 days post-infection, cultures were prepared for electron microscopy as previously described[9].

Immuno-electron microscopy. Samples (either cultured cells or whole brain) were fixed in 4% paraformaldehyde in 0.25 M HEPES for 1 h. Cultured cells were scraped and resuspended in 10% gelatin. Samples were rinsed in PBS, chilled and trimmed to smaller blocks then placed in 2.3 M sucrose overnight on a rotor at 4 °C. Brain tissue was cut into small pieces and placed in 2.3 M sucrose overnight on a rotor at 4 °C. Samples were then transferred to aluminium pins and frozen rapidly in liquid nitrogen. The frozen block was trimmed on a Leica Cryo-EMUC6 UltraCut and 65–75-nm-thick sections were collected using a previously published method[70]. The frozen sections were collected on a drop of sucrose, thawed and placed on a nickel formvar/carbon-coated grid and floated in a dish of PBS ready for immunolabelling. Grids were placed section side down on drops of 0.1 M ammonium chloride for 10 min to quench untreated aldehyde groups, then blocked on 1% fish-skin gelatin in PBS for 20 min. Single-labelled grids were incubated with rabbit anti-Bcl-x (Biocarta; 1:50) before rinsing and using 10 nm protein-A gold (UtrectUMC) for 30 min. Double-labelled grids used the primary rabbit anti-Bcl-x antibody with 10 nm protein-A gold followed by a primary mouse anti-mSod2 (Abnova 1:150) bridged using rabbit anti-mouse (Jackson 1:150) and 5 nm protein-A gold. All grids were rinsed in PBS, fixed using 1% gluteraldehyde for 5 min, rinsed and transferred to a uranyl acetate/methylcellulose drop for 10 min. Samples were viewed with a FEI Tencai Biotwin TEM at 80 kV. Images were taken using a Morada CCD and iTEM (Olympus) software.

Immunoprecipitation and western blot analysis. Cell lysate was incubated with 2 μg rabbit anti-Bcl-x_L (54H6, Cell Signaling) and mouse anti-β-subunit (Mitosciences) antibodies in RIPA (radioimmunoprecipitation assay) buffer overnight at 4 °C with gentle rocking. Protein-G Sepharose beads (Sigma-Aldrich) were added and incubated overnight at 4 °C. Following three washes with the lysis buffer, the bound proteins were eluted from the beads with 2× Laemmli sample buffer. The immunoprecipitated samples were analysed by western blotting. For the Bcl-x_L-synthase interaction study, the human open reading frame constructs for α, β, b, c, δ, d, ϵ, γ and OSCP ATP-synthase subunits, tagged with Myc and DDK (Flag), from Origene Technologies, were expressed in 293T cells and purified, using the EZview Red Anti-FLAG M2 Affinity Gel (Sigma), according to the manufacturer's protocol. The expression was verified and the binding of Bcl-x_L to individual subunits was assessed by immunoblot analysis, using the mouse anti-Myc and rabbit anti-Bcl-x_L antibodies (Cell Signaling), respectively.

Western blotting for mitochondrial protein was carried out using the following antibodies: rabbit anti-human Bcl-x_L (A.G.Scientific, 1:1,000), anti-GFP antibody (ab290, Abcam, 1:1,000), rabbit anti-Drp1 (sc-32898, Santa Cruz, 1:1,000), rabbit anti-VDAC (#4866, Cell Signaling, 1:1,000), mouse anti-GAPDH, (sc-32233, Santa Cruz, 1:1,000), rabbit anti-ANT (sc-11433, Santa Cruz, 1:1,000), rabbit anti-PGC1 α, (#2178, Cell signalling, 1:1,000) and mouse anti-COXIV, (ab14744, abcam, 1:1,000).

Lactate measurements. Lactate was measured by enzyme-controlled fluorometric assay for NADPH–NADP conversion, following a previously published method[71], using a CMA600 analyser (CMA; Microdialysis).

Statistical analysis. For comparisons involving two groups, paired or unpaired Student's *t*-tests (two-tailed) were used. In all figures, $^{*} = P < 0.05$, $^{**} = P < 0.01$ and $^{***} = P < 0.001$ denote significance level, and exact *P* values are provided in the figure legends.

62. Krueger, S. R., Kolar, A. & Fitzsimonds, R. M. The presynaptic release apparatus is functional in the absence of dendritic contact and highly mobile within isolated axons. *Neuron* **40,** 945–957 (2003).
63. Brewer, G. J. Isolation and culture of adult rat hippocampal neurons. *J. Neurosci. Methods* **71,** 143–155 (1997).
64. Lois, C., Hong, E. J., Pease, S., Brown, E. J. & Baltimore, D. Germline transmission and tissue-specific expression of transgenes delivered by lentiviral vectors. *Science* **295,** 868–872 (2002).
65. Komai, S. *et al.* Postsynaptic excitability is necessary for strengthening of cortical sensory responses during experience-dependent development. *Nat. Neurosci.* **9,** 1125–1133 (2006).
66. Buerli, T. *et al.* Efficient transfection of DNA or shRNA vectors into neurons using magnetofection. *Nat. Protoc.* **2,** 3090–3101 (2007).
67. Gajewski, C. D., Yang, L., Schon, E. A. & Manfredi, G. New insights into the bioenergetics of mitochondrial disorders using intracellular ATP reporters. *Mol. Biol. Cell* **14,** 3628–3635 (2003).
68. Lotscher, H. R., deJong, C. & Capaldi, R. A. Inhibition of the adenosinetriphosphatase activity of Escherichia coli F1 by the water-soluble carbodiimide 1-ethyl-3-[3-(dimethylamino)propyl]carbodiimide is due to modification of several carboxyls in the β subunit. *Biochemistry* **23,** 4134–4140 (1984).
69. Nieuwenhuis, F. J., Kanner, B. I., Gutnick, D. L., Postma, P. W. & van Dam, K. Energy conservation in membranes of mutants of Escherichia coli defective in oxidative phosphorylation. *Biochim. Biophys. Acta* **325,** 62–71 (1973).
70. Tokuyasu, K. T. A technique for ultracryotomy of cell suspensions and tissues. *J. Cell Biol.* **57,** 551–565 (1973).
71. Lowry, O.H. & Passoneau, J.V. *A Flexible System of Enzymatic Analysis* (Academic, 1972).

nature cell biology

DOI: 10.1038/ncb2330

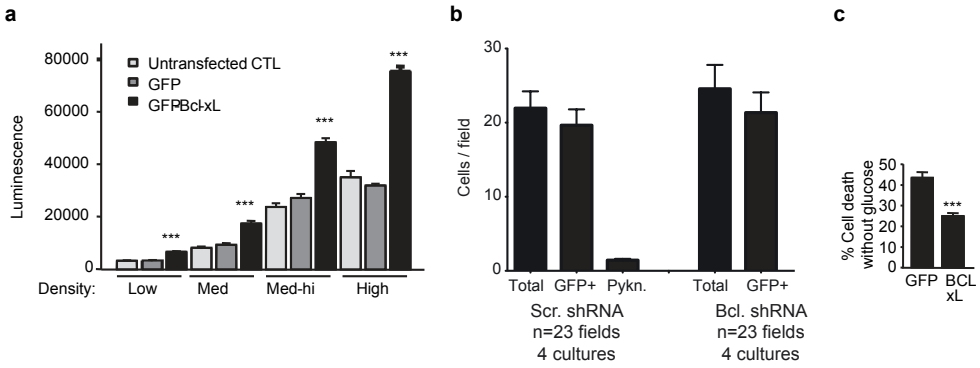

Figure S1 a. ATP levels for different densities of neuron plating; low (n=12 wells for each condition), medium (n=4 wells each condition), medium-high (n=4 wells each condition) and high (n=3 wells each condition); experiments were from two independent cultures (***p< 0.0001 for GFP- Bcl-x_L compared to control or GFP). b. Number of total cells, green fluorescent cells, and green fluorescent cells with pyknotic nuclei (stained with DAPI) per field at 4 d after transduction in cultures of hippocampal neurons transduced with GFP-Bcl-x_L shRNA or scrambled GFP-shRNA (n=23 from 4 cultures per condition). c. Percent cell death of GFP- Bcl-x_L over-expressing cultures vs. GFP expressing cultures in media lacking glucose containing only mitochondrial substrates (5mM methylpyruvate and 5mM methylsuccinate). Dead cells are expressed as a percentage of the total number of cells (one culture; N=14 different plates for each condition of GFP- Bcl-x_L vs. GFP, ***p< 0.0001). For all panels error bars indicate SEM.

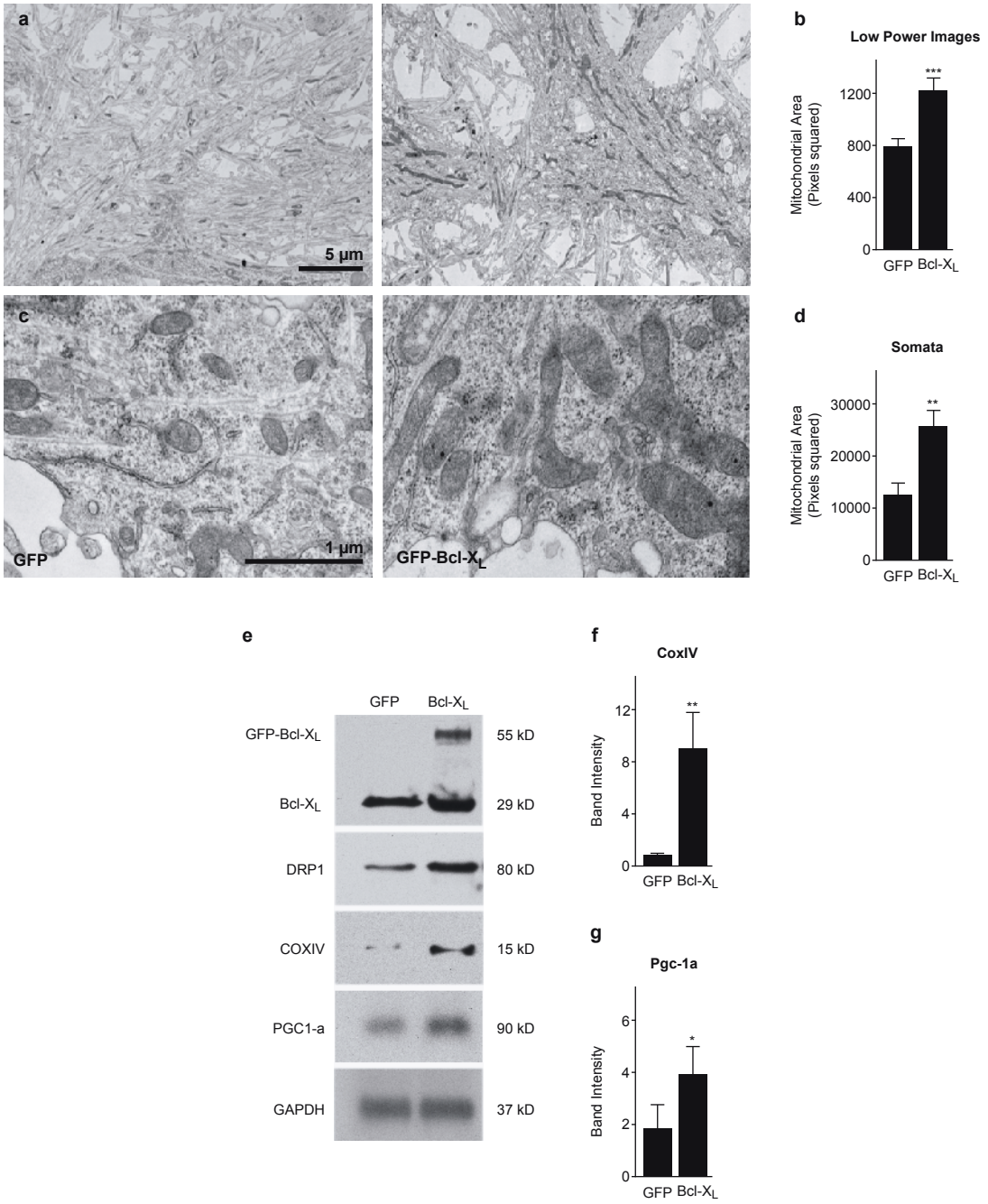

Figure S2 a. Examples of low power electron micrographs of GFP or GFP- Bcl-x_L expressing cultures. b. Group data for total mitochondrial area in low power images of cells in GFP- Bcl-x_L expressing neurons vs. GFP expressing neurons at 7 days after transduction (***p<0.0001, N=2 images for each condition, a total of 673 regions of interest were measured for GFP- Bcl-x_L, 853 for GFP). Mitochondrial area in GFP- Bcl-x_L expressing neurons is approximately 50% increased over controls. c. Examples of high power electron micrographs of somata of GFP or GFP- Bcl-x_L expressing cultures. d. Group data for measurements in somata (**p<0.005, 9 micrographs of GFP, 124 mitochondrial measurements compared to 10 micrographs of GFP- Bcl-x_L, 205 mitochondrial measurements). The data indicate that mitochondria area is increased in the somata, not only in the neuronal processes. e. Cellular protein amounts and amount of a mitochondrial transcription factor. Shown are representative Western blots of cell lysates from GFP or GFP- Bcl-x_L expressing hippocampal cultures. f. Quantification of protein levels for the indicated protein. The optical densities of the bands of proteins from GFP- Bcl-x_L expressing cultures were normalized to the density of a control protein (GAPDH), then expressed as a fold increase over the densities in GFP expressing cultures (N=3 separate cell cultures for each group; **p, 0.02). g. Quantification of protein levels for the indicated protein. The optical densities of the bands of proteins from GFP- Bcl-x_L expressing cultures were normalized to the density of a control protein (GAPDH), then expressed as a fold increase over the densities in GFP expressing cultures (N=3 separate cell cultures for each group; *p, 0.05). The data indicate that mitochondrially-associated proteins are increased in GFP- Bcl-x_L expressing cultures over controls, consistent with mitochondrial biogenesis due to Bcl-x_L over-expression. For all panels error bars indicate SEM.

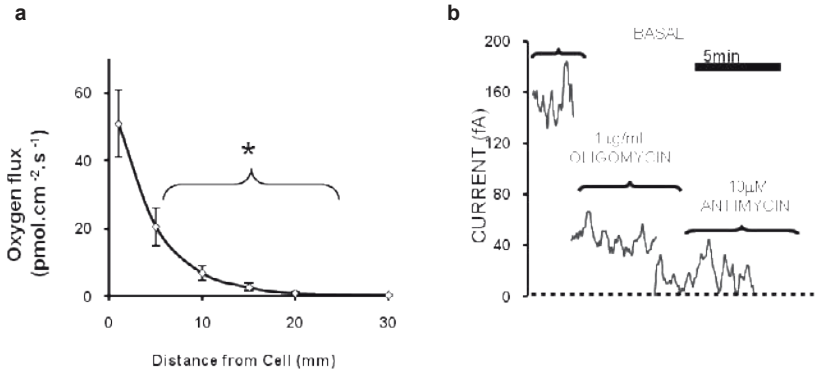

Figure S3 a. Oxygen flux level is indirectly proportional to distance of the oxygen recording electrode from the cell (N=3 cells). Error bars indicate SEM. b. Representative current recording from a self-referencing O_2 sensor. The current is proportional to the O_2 gradient established by a respiring cell, falls after treatment with the ATP synthase inhibitor oligomycin and is almost completely removed with the respiratory chain inhibitor antimycin.

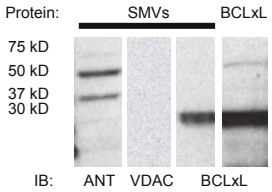

Figure S4 Examples of western blots of purified SMVs immunoblotted with the indicated antibodies. Last lane represents recombinant Bcl-x_L protein.

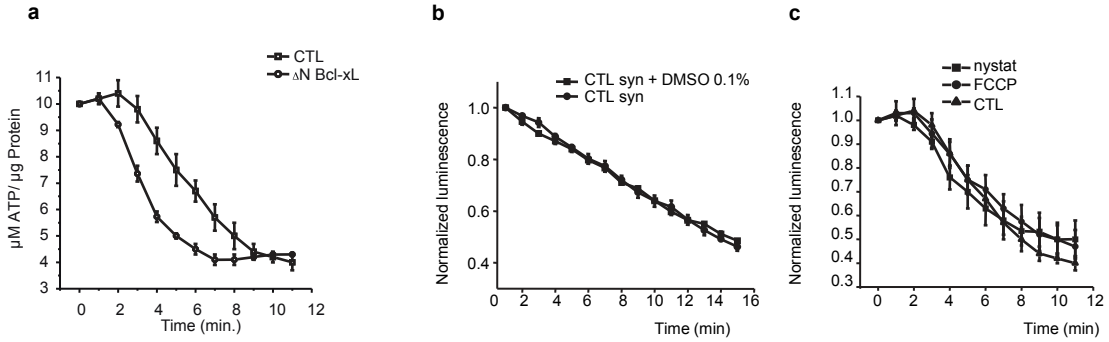

Figure S5 a. Luminescence of firefly Luciferin;luciferase activity in the presence of ATP. N=3 wells F_1F_O ATP synthase plus control protein (0.05mg/ml BSA); N=3 wells F_1F_O ATP synthase plus recombinant deltaN Bcl-x_L protein (1.8mg protein/ml); F_1F_O. ATP synthase concentration for all experiments was 4mg protein/ml). Experiments were repeated and confirmed on 3 different experimental days using at least two different F_1F_O ATPase vesicle preparations (from two different animals). b. F_1F_O ATPase activity in the absence and presence of 0.1% DMSO. Luminescence of firefly Luciferin;luciferase activity in the presence of ATP (N=3 wells in each group. Experiment repeated three times on two different preparations of SMVs with similar results). c. F_1F_O ATPase activity in the absence and presence of FCCP (1µM) and nystatin (10µM). Luminescence of firefly Luciferin;luciferase activity in the presence of ATP (N=3 wells in each group). For all panels error bars indicate SEM.

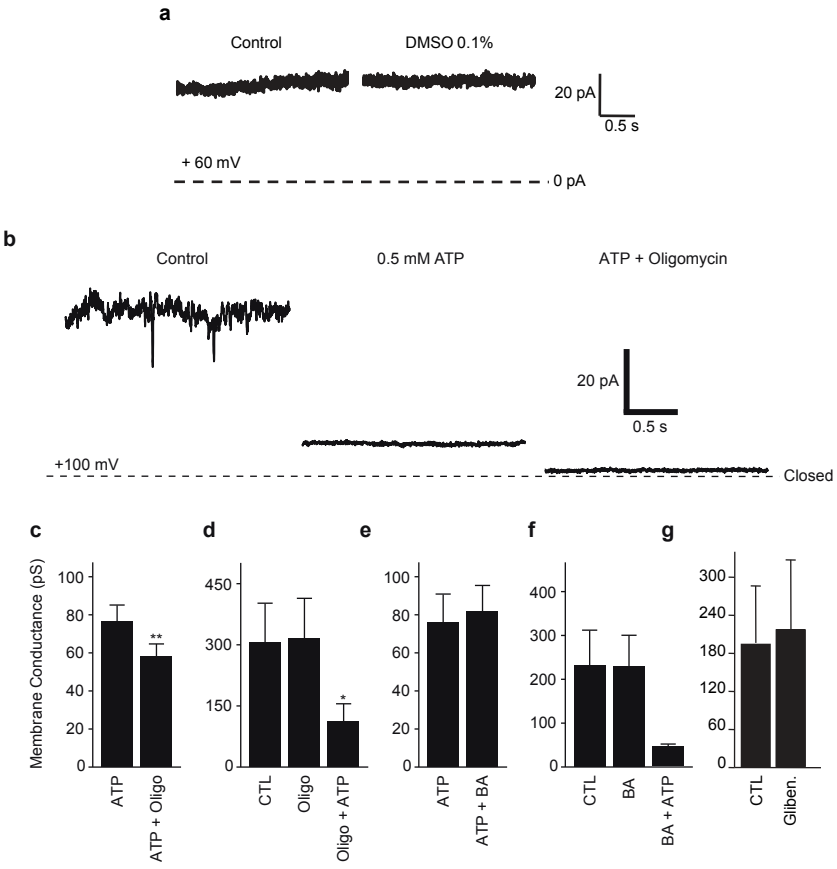

Figure S6 a. Example of SMV patch recording before and after 0.1% DMSO. b. Example SMV recordings before and after ATP, then after oligomycin (5mg/ml final). c. Group data for ATP-exposed SMV patch recordings before and after the addition of oligomycin (N=13 separate SMV recordings before and after oligomycin, **p<0.01, paired t test). Shown is the mean membrane conductance in both conditions after baseline leak subtraction. Because the effect of oligomycin is not occluded by pre-treatment with ATP, the data indicate that the ATP-sensitive conductance in SMVs is different from the oligomycin-sensitive proton conductance. d. Group data for SMV patch recordings before and after the addition of oligomycin, then ATP. Shown is the membrane conductance after baseline leak subtraction (N=7 recordings; *p<0.02). Note that the oligomycin-sensitive conductance is not present in the absence of ATP. e. Group data for ATP-exposed SMV patch recordings before and after the addition of Bongkrekic acid (BA; 10μM final), a membrane permeable inhibitor of ANT. Shown is the membrane conductance in both conditions after baseline leak subtraction (N=6 recordings). The data indicate that the ATP-regulated leak conductance is pharmacologically distinct from that of ANT. f. Group data for SMV patch recordings indicate that ATP is effective after the application of BA (N=6 before and after BA; N=3 to which ATP was added. g. Another conductance of the inner membrane that is sensitive to ATP is that of K_{ATP}. A known inhibitor of K_{ATP} channels, glibenclamide (1μM), had no effect on the conductance of the patches (N=3), suggesting that K_{ATP} was also not responsible for the ATP-sensitive conductance in the F_1F_O ATPase vesicle recordings shown in Figs. 6. For all panels error bars indicate SEM.

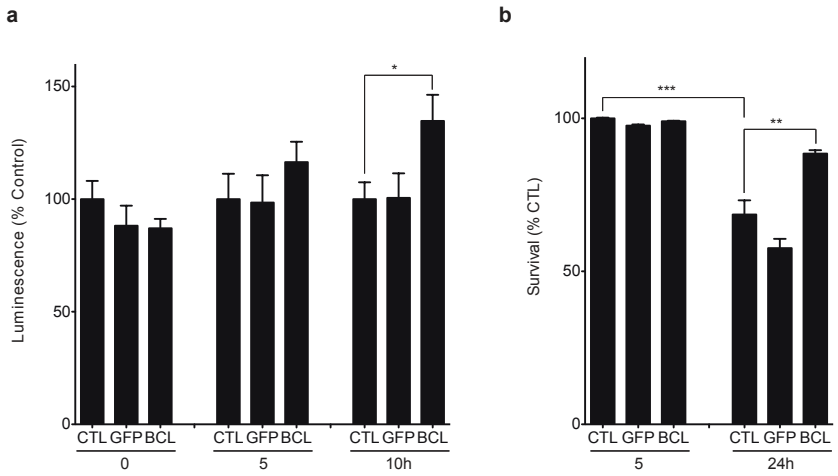

Figure S7 a. ATP levels measured by luminescence of firefly luciferase in Bax-/-;Bak-/- MEFs expressing the indicated constructs measured at 0, 5, 10hrs after change to galactose-containing, glucose-free medium (N=6 wells; *p < 0.05; experiments confirmed by two independent experiments). For each time point, measurements are normalized to the average of the control data. b. Cell survival measured at 5 and 24hrs after switching to galactose-containing, glucose-free medium. MEFs are expressing the indicated constructs (N=7 wells for each condition; **p < 0.01, ***p < 0.001; experiments confirmed by two independent experiments). For all panels error bars indicate SEM.

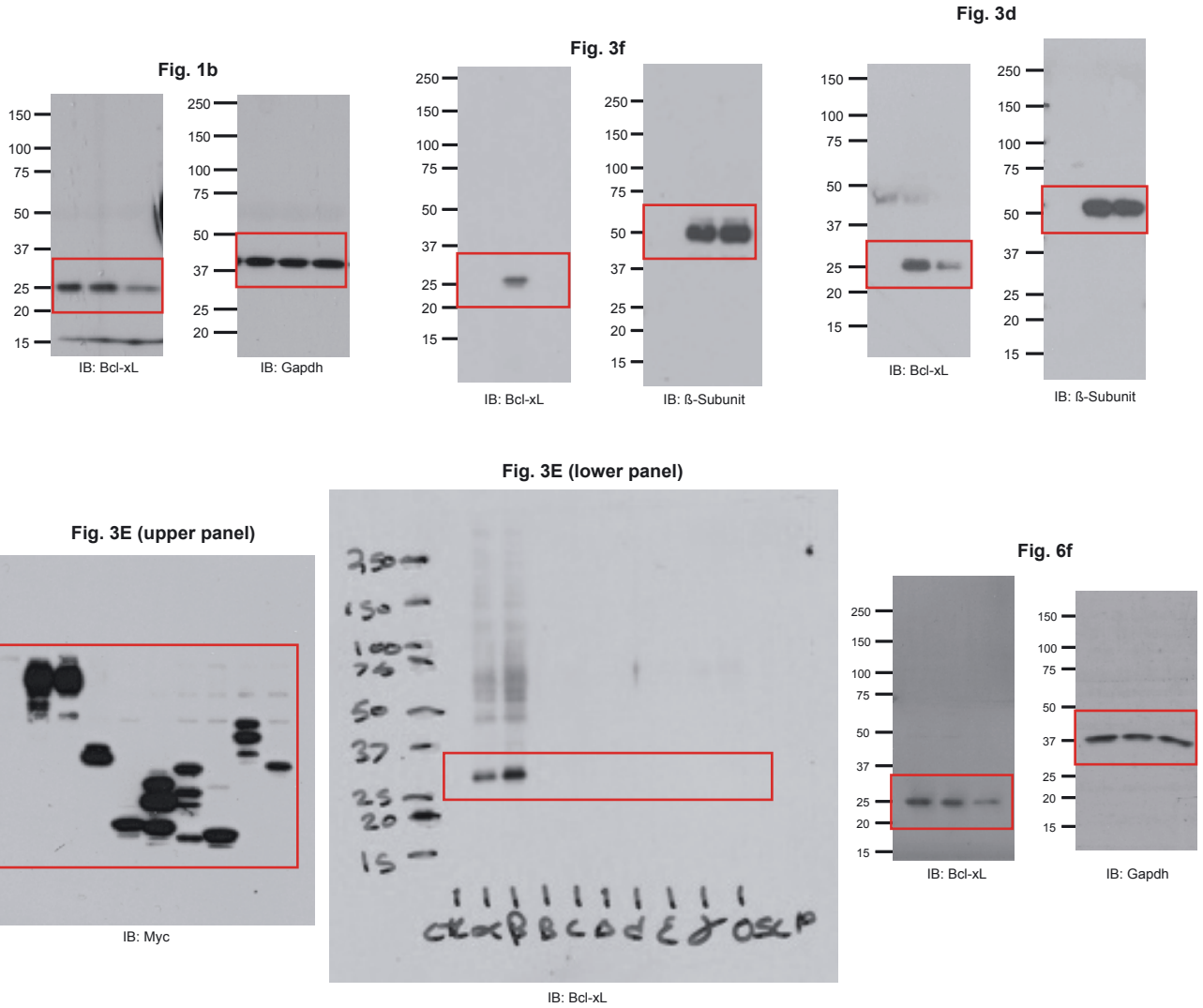

Figure S8 Uncropped images of films for the key experiments in the main figures.